Earth-Science Reviews 203 (2020) 103028

Contents lists available at ScienceDirect

Earth-Science Reviews

journal homepage: www.elsevier.com/locate/earscirev

Continental-scale magnetic properties of surficial Australian soils

Pengxiang Hu[a,*], David Heslop[a], Raphael A. Viscarra Rossel[b], Andrew P. Roberts[a], Xiang Zhao[a]

[a] Research School of Earth Sciences, Australian National University, Canberra, ACT 2601, Australia
[b] School of Molecular and Life Sciences, Faculty of Science and Engineering, Curtin University, GPO Box U1987, Perth, WA 6845, Australia

ARTICLE INFO

Keywords:
Surficial Australian soil
Magnetic properties
Soil forming factors

ABSTRACT

Soil magnetism reflects the physical properties of mainly iron oxide and oxyhydroxide minerals, which provides important information for deciphering soil environments. Establishing national scale soil magnetic databases can provide important reference information that can assist mineral surveying and agricultural planning. Our aims are to provide visualizations and to describe multiple magnetic properties across Australia, to evaluate the relationship between soil magnetism and soil forming factors, and to interpret the mechanisms responsible for surface soil magnetism in Australia. We present the first surficial Australian soil magnetic database, which contains 471 topsoil samples of natural and unpolluted materials. The samples were characterized with detailed magnetic measurements, which show that the magnetic properties of Australian soils vary considerably, but most surficial soils have small concentrations of coarse-grained magnetic minerals. The vast central Australian interior is characterized by weak magnetism, with more hematite and goethite contribution. Strong magnetic hotspots occur in the northwestern plateau, Nullarbor Plain, and eastern highlands. Parent material acts as the dominant control on soil magnetic properties, influencing magnetic mineral concentration and grain size, and controlling the contribution and relative importance of hematite to goethite. Temperature and rainfall both have a weak negative influence on superfine ferrimagnetic particles, due to progressive transformation to hematite and particle migration driven by intensive rainfall in sandy soils. Biota and land use changes tend to have a more complex and integrated local influence on hematite and goethite formation and preservation.

1. Introduction

Soil interacts with the lithosphere, hydrosphere, atmosphere, and biosphere, and is a product of the interactions of climate, topographic relief, organisms, and parent material over time (Jenny, 1941). Soil undergoes continuous development via physical, chemical, and biological processes, including weathering and erosion. Therefore, interpreting soil properties can provide important information on geological, climatic, and environmental processes (Doetterl et al., 2015; Koster et al., 2004; McColl et al., 2017; Paustian et al., 2016; Zamanian et al., 2016). Mapping of soil characteristics provides knowledge of spatial soil variations that have important implications for land management, archaeology, mineral prospecting, and theoretical and applied soil science (Ballabio et al., 2016; Brevik et al., 2016; Chaney et al., 2016; Draper et al., 2009; Hartemink et al., 2013; Hengl et al., 2015, 2017; Jafari et al., 2013; Lee et al., 2006; McBratney et al., 2003; Rachwał et al., 2017; Viscarra Rossel, 2011; Viscarra Rossel et al., 2015; Zeraatpisheh et al., 2017). Establishment of soil databases is also important for modelling soil functions and to reveal the role of soil forming factors on different spatial and temporal scales (Batjes, 2016; Blundell et al., 2009a; Gray et al., 2009; Orgiazzi et al., 2018; Viscarra Rossel et al., 2016).

Soil magnetism mainly reflects the type, concentration, and size distribution of iron oxides and oxyhydroxides, which are essential to soil properties, such as colour, cation and anion retention, particle aggregation, and electron and proton buffering, even when present in small concentrations (Colombo et al., 2014; Cornell and Schwertmann, 2004; Torrent et al., 1980; Viscarra Rossel et al., 2010). Iron oxides in soil usually have multiple origins, and are sensitive to soil conditions, including parent material, pH, redox potential, moisture, microbial activity, as well as anthropogenic activities, natural fire, and climatic conditions. Soil magnetism is, therefore, an important topic in earth and environmental science (Blundell et al., 2009a; Dearing et al., 1996; Heller and Evans, 1995; Jordanova, 2017; Liu et al., 2007, 2012; Maher, 1998), and can be indicative of sediment source (Bloemendal et al., 1988; Dearing, 1999, 2000; Hatfield and Maher, 2008; Manjoro et al., 2017; Pulley et al., 2018), vegetation change (Maxbauer et al., 2017), soil erosion and degradation (Ayoubi et al., 2012; Carcaillet et al., 2006; Foster et al., 2000; Jordanova et al., 2011b; Mokhtari Karchegani et al., 2011; Sadiki et al., 2009), paleoenvironmental

* Corresponding author.
E-mail address: pengxiang.hu@anu.edu.au (P. Hu).

https://doi.org/10.1016/j.earscirev.2019.103028
Received 26 February 2019; Received in revised form 8 November 2019; Accepted 8 November 2019
Available online 21 November 2019
0012-8252/

changes (Ahmed and Maher, 2018; Gao et al., 2018; Hu et al., 2015; Liu et al., 2013; Lyons et al., 2010, 2014; Maher, 1998; Maher et al., 2002, 2003; Maxbauer et al., 2016; Torrent et al., 2010), pollution detection (Ayoubi et al., 2018; Ayoubi and Karami, 2019; Blundell et al., 2009b; Chaparro et al., 2006; Hanesch and Scholger, 2002; Hoffmann et al., 1999; Martin et al., 2018; Naimi and Ayoubi, 2013), and anthropogenic activity (Dalan and Banerjee, 1996; Dankoub et al., 2012).

The most debated topic in soil magnetism concerns the mechanisms of magnetic mineral formation and preservation, and the influence of soil forming factors, which are fundamental to the use of soil magnetic properties for paleoenvironmental reconstructions. As discussed extensively in the literature, the 'fermentation' mechanism (Le Borgne, 1955; Mullins, 1977), competitive abiotic magnetite formation (Maher, 1998; Maher and Taylor, 1988), fire and thermal transformation of weakly magnetic iron minerals to ferrimagnetic minerals (Kletetschka and Banerjee, 1995; Le Borgne, 1960; Oldfield and Crowther, 2007), pedogenic bacterial magnetosome production (Fassbinder et al., 1990), and abiotic aging of ferrihydrite to hematite through intermediate maghemite have been proposed to explain soil magnetism (Barrón et al., 2003; Hu et al., 2013; Jiang et al., 2018; Liu et al., 2008; Michel et al., 2010; Torrent et al., 2006). The five soil forming factors (Jenny, 1941) have also been studied intensively (Blundell et al., 2009a). Climate, particularly rainfall, has received the most attention (Balsam et al., 2011; Geiss and Zanner, 2007; Han et al., 1996; Heslop and Roberts, 2013; Liu et al., 2013; Maher and Thompson, 1995; Maher et al., 2002; Maher and Possolo, 2013; Maher and Thompson, 1992; Maxbauer et al., 2016) and has been proposed to drive hydrolysis reactions and Fe release from primary minerals, which results in higher magnetic susceptibility values (Maher and Thompson, 1995; Singer et al., 1996). However, the relationship between rainfall and magnetic properties in soils is complicated by increased magnetic mineral dissolution at a rainfall threshold of around 1000 to 1500 mm/yr (Balsam et al., 2011; Long et al., 2011), where soil moisture ultimately controls the chemical reactions that form or dissolve soil magnetic minerals (Guo et al., 2001; Hu et al., 2015; Orgeira et al., 2011). Parent material is also considered essential for magnetic mineral production by influencing Fe supply, igneous rock weathering, and local soil conditions (Blundell et al., 2009a; Jordanova et al., 2016). The effects of relief and drainage, soil organisms, and time are less well studied in relation to soil magnetism. The few studies that address these factors indicate that relationships are complicated by local soil conditions, including, for example, particle size and the activity of dissimilatory iron reducing bacteria (DIRB) (Dearing et al., 1996; Hannam and Dearing, 2008; Thompson and Oldfield, 1986).

An effective way to test the mechanisms that control soil magnetism and the effects of soil forming factors is by using large scale data sets, as has been done in England and Wales, Austria, Bosnia-Herzegovina, and Bulgaria (Blundell et al., 2009a, 2009b; Dearing et al., 1996; Hanesch et al., 2007; Hannam and Dearing, 2008; Jordanova et al., 2016; Rachwał et al., 2017). Surficial soil magnetic maps generated through such work are essential for soil evaluation (Jordanova et al., 2016), detecting pollution (Blundell et al., 2009b; Dearing et al., 1996; Hanesch et al., 2007; Rachwał et al., 2017), and land management (Hannam and Dearing, 2008). Most importantly, such studies provide a statistical framework to enable predictive modelling of soil magnetism in relation to the soil forming factors.

The first conceptual model of secondary ferrimagnetic mineral formation in temperate regions was constructed by investigating magnetic susceptibility and frequency-dependent susceptibility maps of topsoils across England (Dearing et al., 1996). From this model, large-scale first-order factors, climate and parent material, combine to control soluble Fe flux and ferric (oxyhydr-)oxide production in soils. At local scales, vegetation, land use, and relief influence pedogenic formation and accumulation of ferrimagnetic minerals. Blundell et al. (2009a) published a comprehensive and detailed statistical analysis of magnetic susceptibility and frequency-dependent susceptibility of topsoils across England and Wales and reviewed the role of soil forming factors on their spatial patterns. They concluded that parent material and drainage are the dominant factors that affect soil magnetic susceptibility, while rainfall, relief, land use, organic carbon, and pH have a lesser effect, while time and temperature do not play a significant role in controlling soil magnetic susceptibility. Jordanova et al. (2016) developed a Bulgarian database of topsoil magnetic properties. The spatial distribution of magnetic susceptibilities is related to surface geology, which indicates that parent material has a dominant influence on magnetic mineralogy. Climatically driven pedogenic magnetic enhancement of soils that developed on strongly magnetic volcanic and intrusive rocks is affected mainly by rainfall, while for soils developed on loess, marls, and limestone, increased frequency-dependent susceptibility is related to temperature. However, all studies so far have been made on European soils from temperate climates and most have significant anthropogenic influences. Data from other regions are needed to better understand the complexity, mechanisms, and potential applications of soil magnetism.

As the oldest, flattest, and driest inhabited continent, the geology, landscape, vegetation, and climate of Australia are unique. Australia's size gives it diverse landscapes, with tropical rainforests in the northeast, mountain ranges in the southwest and east, and dry deserts in the centre. Parts of the continent have been exposed to sub-aerial conditions for over one billion years, so rocks exposed at the surface have experienced a wide range of climates and tectonic events, which have caused variable chemical and physical environments that have resulted in intense weathering (Anand, 2005). Australian soils have not been replenished by glaciers for 300 million years, so many soils have continued to weather over exceptionally long periods. Sandy soils with clay contents < 20% cover vast areas of western and central Australia; these soils have low water-holding capacity and drain rapidly to the water table (The Soil and Landscape Grid of Australia, http://www.clw.csiro.au/aclep/soilandlandscapegrid/index.html, Grundy et al., 2015; Viscarra Rossel et al., 2015). Australian geology, climate, and the nature of Australian soils provide an opportunity to develop a soil magnetism data set to investigate the influence of soil forming factors.

Few magnetic investigations have been made on Australian soils. The magnetic properties of some soil types have been studied to identify sediment sources in water bodies for erosion studies (Crockford and Fleming, 1998; Crockford and Olley, 1998; Crockford and Richardson, 2004; Crockford and Willett, 1995, 2001). These studies indicate that diagenesis and drying affects soil magnetic properties by forming complex iron oxides during reduction that are then destroyed by oxidation (Crockford and Willett, 1995). Abrasion and breakage of particles during transportation also have a substantial influence on iron and magnetic mineral concentrations in soils, but their effects vary with soil type (Crockford and Olley, 1998). Fire enhancement (high temperatures with reducing conditions), aggregation and de-aggregation of maghemite, partial dissolution of maghemite under the influence of organic matter and hydromorphy, are documented mechanisms responsible for causing magnetic property changes along a soil profile in New South Wales (Crockford and Willett, 1997). From analysis of a Yellow Dermosol (Isbell, 2016) profile near Canberra, Crockford and Willett (2001) concluded that fire enhancement of maghemite was responsible for surface soil magnetism and that coarser lithogenic particles generally have stronger magnetism. They also argued that large Al concentrations might minimize maghemite concentration to favour goethite and hematite production. From analysis of a loess profile in New South Wales, Ma et al. (2013) suggested that the weak magnetism of the Mackenzie's Waterholes Creek loess (the deepest and first dated loess profile in New South Wales) compared to typical Chinese loess sequences is probably due to reducing conditions associated with excessive soil waterlogging.

Previous magnetic studies reveal the distinctiveness of Australian soil magnetism due to geology and climate. However, considering the variable geology and climate across such a vast continent, more

systematic analysis is needed to understand Australian soil magnetism at a continental scale. Viscarra Rossel et al. (2010) published the first iron oxide map of Australian surface soils using visible–near infrared reflectance spectra, which provides estimates of the relative abundance of hematite and goethite. As the "red continent", soils in large parts of western and central Australia are dominated by hematite, while goethite is dominant in eastern Australia, southwestern Western Australia, and western Tasmania. Climate exerts a strong influence on the hematite/goethite ratio, and ion activity and soil organic matter also have an influence. Goethite is favoured in lower parts of the landscape where reducing conditions can occur with acidic pH, high H_2O and Al activities, and more organic matter. Hematite is prevalent in higher parts of the landscape with hot and arid climates and more alkaline pH.

Pioneering magnetic studies on national soil datasets from various countries have contributed significantly to understanding of soil forming factors on surface soil magnetism. Magnetic investigation of Australian soils should also, therefore, provide a valuable reference point for interpreting the magnetism of Australian soils and their relationship with climate and geological factors. In this paper, we first review previous magnetic studies of various national soil collections and then provide the first magnetic analysis of an Australian national soil collection. We use our magnetic database to derive maps that describe continental-scale magnetic property variability across Australia and evaluate the significance of soil forming factors on that distribution. From that base, we propose a first conceptual model of Australian soil magnetism.

2. Materials and methods

2.1. Materials

The studied surface soil samples are from a selected subset of specimens from the National Soil Archive of the Australian Commonwealth Scientific and Industrial Research Organization (CSIRO) (Viscarra Rossel et al., 2010; Viscarra Rossel, 2011) and the National Geochemical Survey of Australia (NGSA) (de Caritat and Cooper, 2011, 2016). Samples from NGSA were collected from catchments and sampled at 0–10 cm below the surface (below the root zone, if applicable). To reduce natural soil heterogeneity, every sample collected was a composite either from a shallow soil pit or from at least three auger holes. All samples were air-dried, homogenized, and archived (de Caritat and Cooper, 2016). Samples from depths of 0–20 cm were also obtained from the CSIRO National Soil Archive (Viscarra Rossel et al., 2010). These samples provide a fairly even representation of landforms across Australia (see details in Viscarra Rossel et al., 2019, supplementary material, 'the dataset used' section).

We analyzed 497 topsoil samples, which are representative of the range of Australian soil classification orders (Isbell, 2016) and climatic regimes across Australia (Fig. 1a). All samples, in an air-dry condition, were placed into 2 cm × 2 cm × 2 cm plastic boxes for magnetic measurements (Fig. 1b). Clay minerals, colour, iron oxides, organic carbon stocks, and other functional soil properties of Australian soils have been well studied (Viscarra Rossel, 2011; Viscarra Rossel et al., 2010, 2014; Viscarra Rossel and Webster, 2012), and provide important background information for environmental magnetic studies.

2.2. Magnetic measurements

Mass-specific magnetic susceptibility (χ) was measured using a Bartington Instruments MS2 magnetic susceptibility meter at dual frequencies of 470 Hz (χ_{LF}) and 4700 Hz (χ_{HF}). The absolute frequency-dependent magnetic susceptibility is defined as $\chi_{FD} = \chi_{LF} - \chi_{HF}$, and the relative frequency-dependent magnetic susceptibility, $\chi_{FD\%}$ is calculated as $100 \times \chi_{FD}/\chi_{LF}$. An ARM was imparted in an alternating field (AF) of 80 mT with a superimposed 50 μT bias field and is expressed in terms of.

ARM susceptibility (χ_{ARM} = ARM/bias field). ARM was then AF demagnetized in 40 steps from 2.5 mT to 125 mT with logarithmically spaced fields; the medium destructive field of ARM (MDF_{ARM}) was calculated from such demagnetization curves. An IRM was imparted in a 2.5 T field, which is referred to as the 'saturation' IRM ($SIRM_{2.5T}$), which was demagnetized in 40 logarithmically spaced AFs from 2.5 mT

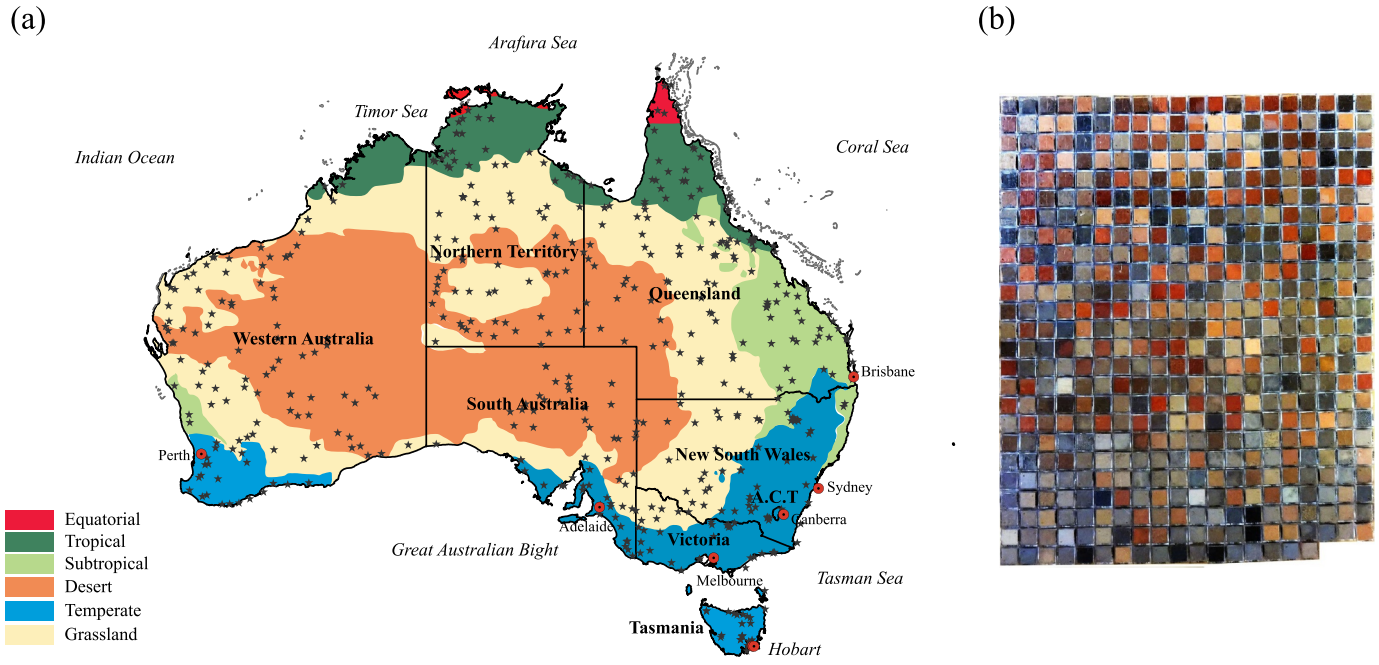

Fig. 1. (a) Spatial distribution of soil sample locations (stars). (a) The background map is the Köppen classification map with six major groups across Australia from the Bureau of Meteorology, Australian Government (http://www.bom.gov.au/jsp/ncc/climate_averages/climate-classifications/index.jsp?maptype=kpngrp#maps). (b) Photograph of the samples used in this study. Samples are arranged according to magnetic susceptibility values, where susceptibility decreases from the top left to bottom right.

to 125 mT. The medium destructive field of IRM (MDF_{IRM}) was calculated from such demagnetization curves. The ratio of the 'hard' IRM after AF demagnetization at 100 mT to $SIRM_{2.5T}$ ($IRM_{AF100\ mT}$/$SIRM_{2.5T}$) is calculated as $HIRM_{AF100}$ to reflect the relative contribution from magnetic minerals with coercivity of remanence (B_{cr}) larger than 100 mT. A backfield of 300 mT was also imparted to the $SIRM_{2.5T}$ to highlight contributions from high-coercivity hematite and goethite. The traditional HIRM proxy, referred to here as $HIRM_{-300mT}$, was calculated as ($SIRM_{2.5T}$ + IRM_{-300mT})/2 and the S-ratio is represented by $-IRM_{-300mT}/SIRM_{2.5T}$ (Liu et al., 2007). Parameters such as χ_{ARM}/χ, ARM/SIRM, and SIRM/χ can be calculated to provide further information about relative magnetic particle size variations (see Liu et al. (2012)). All remanences were measured using a 2-G Enterprises Model 760 cryogenic magnetometer and all magnetic measurements were made at the Black Mountain Paleomagnetism Laboratory, Australian National University, Canberra.

2.3. Unmixing of ARM and $SIRM_{2.5T}$ demagnetization curves

ARM and $SIRM_{2.5T}$ demagnetization curves for 497 samples were processed using the parametric end-member (EM) analysis algorithm of Paterson and Heslop (2015). This algorithm is designed for sediment grain size data, but the unmixing principle is the same for demagnetization data. Demagnetization data was unmixed using the AnalySize package (https://www.github.com/greigpaterson/AnalySize). This decomposition process enables isolation of magnetic components with different coercivities. Coercivity distributions were modelled with a linear combination of skewed generalized Gaussian (SGG) functions (Egli, 2003). We fitted demagnetization curves with up to 5 components and compare the coefficient of determination (R^2) for each number of fits in Fig. 2a, b. Increasing the number of components naturally leads to a better fit; however, it also increases the complexity of solutions.

2.4. Geological, climatic, and geochemical data

Relief was calculated from Shuttle Radar Topography Mission (SRTM) elevation data with a cell size of approximately 90 m. Runoff is the mean annual runoff for 1980–1999, which is calculated as Rainfall + Irrigation - Evaporation. Mean Annual Temperature (MAT) and Mean Annual Precipitation (MAP) were inferred from the Bioclim (ANUCLIM 5.0) software, with Version 2 of the 9-second digital elevation model as the elevation surface. The clay content, available soil water content (AW), pH, and organic carbon (OC) of Australian soil from the upper 0–30 cm layer is from Australia-wide digital soil maps (Viscarra Rossel et al., 2015) of the Soil and Landscape Grid of Australia (http://www.clw.csiro.au/aclep/soilandlandscapegrid/GetData.html). Soil saturated hydraulic conductivity (SHC) data are held in the Australian Soil Resource Information System (ASRIS) (http://www.asris.csiro.au/mapping/viewer.htm). Information about bedrock and regolith cover are sourced from the National Geoscience Database of Australia under the Creative Commons Attribution 4.0 International license. Australia is divided into 392 regolith terrain units based on dominant topography, geology, and regolith in the Regolith Terrains of Australia database (https://data.gov.au/dataset/regolith-terrains-of-australia-national-geoscience-dataset). Bedrock data are from the Surface Geology of Australia (2012 Edition) at 1: 2,500,000 scale under the same license (https://data.gov.au/dataset/surface-geology-of-australia-data-package-2012-edition). Land use types are summarized from The Australian Land Use and Management Classification system (version 3) (http://www.agriculture.gov.au/abares/aclump/land-use/alum-classification).

Soil samples are classified on the order level based on the Australian Soil Classification (Isbell, 2016), which includes Anthroposols, Organosols, Podosols, Vertosols, Hydrosols, Kurosols, Sodosols, Chromosols, Calcarosols, Ferrosols, Dermosols, Kandosols, Rudosols, and Tenosols.

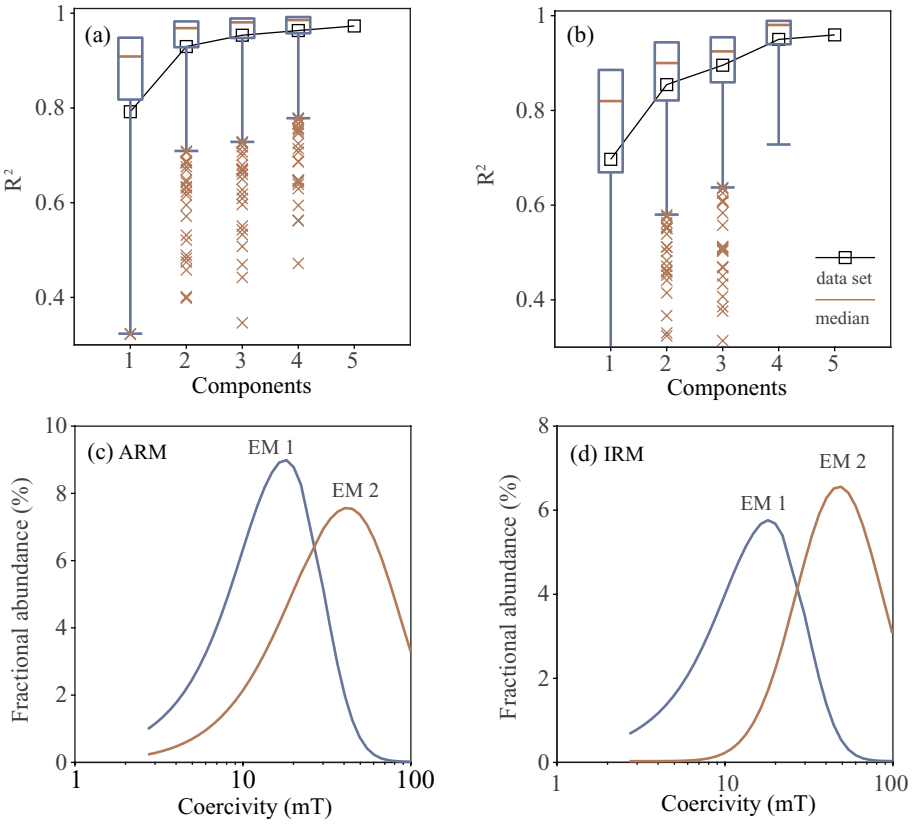

Fig. 2. (a, b) Coefficient of determination (R^2) for 1 to 5 EMs for unmixing of ARM and IRM demagnetization curves using SGG functions for each component. (c, d) SGG EM coercivity distributions for ARM and IRM demagnetization curves.

The Australian Soil Classification is one of the most challenging to correlate with the World Reference Base for Soil Resources (WRB). The main issue is that many soils in Australia have no global counterparts and, thus, are not represented in other classification schemes. Correlations of Australian soil taxa to the WRB are, however, available down to the great group level (Krasilnikov et al., 2009) (Table S1). The spatial distribution of Australian soil classification is shown in Fig. S1. Sodosols are mainly distributed in mountains and plateaus, while central and western Australia are dominated by rudosols and tenosols, which lack pedological organization. Calcarosols are one of the most widespread and important soils in southern Australia.

The normalized Fe oxide difference index (NIODI), which represents the relative abundance of goethite and hematite, is derived from Viscarra Rossel et al. (2010). Positive values indicate greater goethite contributions, while negative values indicate relatively more hematite. Exact diffuse reflectance visible–near infrared spectra wavelength minima and corresponding continuum-removed spectrum reflectance values for windows between 860 nm and 930 nm are assigned as the hematite abundance, while values for windows between 910 nm and 970 nm are assigned as the goethite abundance. Major element concentrations of K, Ca, Fe, Si, and Ti were measured with a P-XRF (Amptek, Bedford, MA, USA), which consists of an Amptek® Mini-X X-ray tube system and an Amptek® X-123 spectrometer. A detailed description of these instruments is provided by Sacristán et al. (2016). Measurement times of 2 min were used and three replicate measurements were made for each sample.

2.5. Statistical analyses and magnetic maps

Only 471 of the studied samples yielded reliable data. Data for these 471 samples were analyzed statistically using principal component analysis (PCA) and Spearman correlation analysis. Maximum, minimum, standard deviation, median, skewness, and kurtosis values were calculated for the whole dataset (Table 1). For category factors, such as parent material, land use and age, the category median value for selected magnetic proxies were calculated and ranked. The correlation coefficient of category median magnetic data versus individual sample magnetic data are examined to reveal association strength. Before conducting PCA, the data set was standardized by z-score. To produce maps of soil magnetic parameter variations, additional data processing steps were followed. First, outlier analysis was performed quantitively using the Cook's distance method (Cook, 1977, 1979). Then, a log-normal transformation or power function was used when necessary to convert highly skewed data into approximately normal distributions.

Ordinary kriging is a geostatistical prediction method for spatial interpolation that uses information from certain regions to estimate values in unsampled locations. The first step is to test the spatial relationship of a given parameter, e.g., whether observations are distributed randomly in a sampled area or whether they are more similar to other nearby values. We use the Global Moran's I index, where its significance is calculated to test spatial autocorrelation of selected parameters (Table S2). The *p*-values of four parameters are statistically significant at the 0.01 confidence level and all z-scores are positive, which indicates that the spatial distribution of high and/or low values in the dataset is more clustered spatially and is not distributed randomly. The first ordinary kriging step involves building an empirical semivariogram. The semivariance gives a quantitative estimate of the spatial behaviour of a given property and is calculated as (Goovaerts, 1997; Oliver and Webster, 2014):

Table 1
Summary statistics for the datasets discussed in the main text.

Parameters	Maximum	Minimum	Standard deviation	Median	Skewness	Kurtosis
χ (10^{-8} m^3/kg)	3922.1	1.3	292.7	40.9	7.1	70.8
χ_{FD} (10^{-8} m^3/kg)	239.4	0.0	17.8	2.3	6.8	68.8
ARM (10^{-6} Am^2/kg)	7235.3	2.5	485.5	80.2	8.1	98.0
SIRM (10^{-4} Am^2/kg)	4727.6	1.2	347.2	35.4	9.1	101.2
$HIRM_{-300}$ (10^{-4} Am^2/kg)	164.9	0.0	15.5	3.2	5.7	42.2
$\chi_{FD\%}$	18.0	0.0	3.4	6.5	0.0	-0.46
ARM/SIRM (10^{-3})	182.6	0.7	16.7	22.1	3.2	21.6
χ_{ARM}/χ	24.0	0.2	2.4	4.9	1.7	9.5
SIRM/χ (10^3 A/m)	58.2	1.1	6.1	8.7	3.5	19.6
$HIRM_{AF100}$ (%)	78.0	1.4	11.5	18.1	1.2	2.4
S-ratio	1.0	-0.2	0.1	0.9	-2.8	12.2
MDF_{ARM} (mT)	42.7	8.6	4.2	16.8	2.1	7.3
MDF_{IRM} (mT)	435.4	8.2	29.0	20.5	7.9	92.3
ARM_{EM1} (%)	100.0	0.0	21.5	80.1	-1.1	1.1
ARM_{EM2} (%)	100.0	0.0	21.5	19.9	1.1	1.1
IRM_{EM1} (%)	100.0	16.7	15.6	84.9	-1.2	1.1
IRM_{EM2} (%)	83.3	0.0	15.6	15.1	1.2	1.4
NIODI index	1.0	-0.3	0.4	0.0	0.8	-0.4
Relief (m)	253.0	5.0	40.7	107.0	0.8	0.1
Runoff (mm)	2653.2	0.1	277.5	25.7	4.3	25.2
Temperature (°C)	27.7	5.0	4.5	21.2	-0.6	-0.2
Rainfall (mm)	4095.0	110.0	491.3	437.0	3.2	15.0
pH	7.9	4.0	0.8	5.7	0.3	-0.6
SHC (10^{-3} mm/hr)	575.5	0.1	113.5	97.5	0.7	-0.6
AW (mm)	0.2	0.1	0.0	0.1	-0.4	1.1
OC (%)	5.6	0.3	0.9	0.8	2.3	6.0
Clay (%)	57.3	8.8	10.1	22.2	0.9	0.2
Sand (%)	58.0	24.2	6.3	44.1	-0.2	-0.4
K (%)	3.6	0.0	0.6	1.3	0.2	-0.4
Fe (%)	9.3	0.7	1.4	2.6	1.4	3.1
Si (%)	53.5	2.4	8.7	31.6	-0.5	1.2
Ca (%)	32.7	0.9	2.9	1.3	7.1	60.1
Ti (%)	3.5	0.0	0.4	0.4	3.5	20.6

$$\gamma(h) = \frac{1}{2N(h)}\left\{\sum_{i=1}^{N(h)} [Z(x_i + h) - Z(x_i)]^2\right\}$$

where $\gamma(h)$ is the semivariance for the range of distances h, $N(h)$ is the number of pairs of observations at distance h, $Z(x_i)$ is the value of the variable at the ith location, and $Z(x_i + h)$ is the value of the variable at location $(i + h)$.

Experimental variograms are approximated analytically to describe the main spatial structures of a variable (McBratney and Webster, 1986; Oliver and Webster, 2014). Experimental variograms were modelled for variables transformed to be approximately normally distributed. The range of values in variograms represents the scale of variation for each mapped parameter.

We do not discuss the large area in and around the Great Sandy Desert and Great Victoria Desert where we have no data. Kriging is not an exact interpolation method, so caution should be exercised when considering data at the edges of this area. Given the vast size of Australia, our limited sample set will inevitably result in significant uncertainties in the maps. Therefore, we illustrate the measured data for each location using graduated symbols on the maps, which represent the original values of the mapped parameters. Maps presented here should not be used as predictive maps for specific locations; a larger database is needed to improve mapping accuracy, although the presented maps provide a reasonable large-scale view of spatial magnetic property distributions.

The Kruskal-Wallis Test is a non-parametric method for testing whether samples from different groups originate from the same data distribution, and is used to test whether magnetic properties from different groups of parent materials, land use, and bedrock geological age differ significantly. If the test result is significant, multiple comparisons will be made between each group to show which two groups differ significantly.

3. Results

3.1. Coercivity EMs of Australian soils

Decomposition of demagnetization curves indicates that 2 end-member components explain > 85% of variance in the ARM and IRM data sets. Coercivity distributions for these components are illustrated in Fig. 2c, d. Four parameters that characterize these coercivity distributions are summarized in Table 2 (median destructive field (MDF), standard deviation (i.e. the dispersion parameter (DP)), and the skewness and kurtosis of each SGG distribution). EM1 for ARM and IRM (MDF ~13 mT, DP ~0.27) is a low coercivity ferrimagnetic component, probably magnetite or maghemite with size just above the superparmagnetic/single domain (SP/SD) threshold and/or coarse detrital (titano-) magnetite in the multidomain (MD) state. EM2 has higher coercivity; for IRM it has a high MDF (~44 mT) and narrower dispersion (~0.22) compared to ARM (MDF ~31 mT, DP ~0.33). Three factors could give rise to the high coercivity of EM2. First, larger SD ferrimagnetic minerals have high coercivity (Butler and Banerjee, 1975; Dunlop and Özdemir, 1997; Li et al., 2017); second, oxidized magnetite has high coercivity due to high internal stresses caused by the unit cell mismatch between the oxidized maghemite rim and the magnetite core of particles (Cui et al., 1994; Ge et al., 2014; Liu et al., 2003; van Velzen and Dekkers, 1999); and third, imperfect antiferromagnetic minerals with high coercivity, such as hematite and goethite, have high bulk coercivity. Considering the huge magnetic property variations in Australian surface soils (see below), variable magnetic mineral types and coercivity distributions are expected. Therefore, both EM1 and EM2 are likely to represent magnetic mineral mixtures with different coercivity distributions. Here, we assign EM1 as a magnetically soft component and EM2 as a magnetically harder component, recognizing that they are likely to have different mineralogical carriers in different soils.

Table 2
Statistical summary of coercivity end members from ARM and IRM demagnetization curves for 471 samples.

		MDF (mT)	DP	Skewness	Kurtosis
ARM	EM1	12.70	0.27	−0.20	2.76
	EM2	30.50	0.33	−0.69	2.86
IRM	EM1	12.90	0.28	−0.21	2.73
	EM2	44.20	0.22	−0.70	3.29

3.2. Statistics for magnetic properties of Australian soils

Descriptive statistics for the magnetic database developed in this paper are given in Table 1. All magnetic properties vary over a large range of values in our sample collection, as indicated by large standard deviations. χ, ARM, and SIRM variations span 3 orders of magnitude from ~0 to several thousands, while χ_{FD}, $SIRM_{AF100}$, $HIRM_{-300}$, and ARM/SIRM range over 2 orders of magnitude with minimum values close to 0, which suggest enormous changes in concentration of both ferrimagnetic and imperfect antiferromagnetic minerals and their grain size distributions. S-ratios vary from negative values to 1 and $HIRM_{AF100}$ ranges from 1% to 78%, which indicates that the relative proportion of imperfect antiferromagnetic minerals changes significantly. These minerals can, therefore, make either minor or major contributions to remanence. Coercivity also undergoes large changes, as suggested by MDF_{ARM} and MDF_{IRM} values. The relative proportions of soft and hard magnetic components also vary greatly, as indicated by the ARM and IRM EMs. Relative hematite and goethite contributions range from nearly all goethite to a preference for hematite is suggested by NIODI index values from −0.3 to 1, which is also reflected by the variable colour of samples from grey-white to dark red and brown-black (Fig. 1b). Descriptive statistical results are also calculated for geographical, soil chemical, and geochemical factors (Table 1), which all indicate large variance among samples.

Histograms of selected magnetic properties (Fig. S2), and the skewness and kurtosis of magnetic property distributions (Table 1), indicate that most measured magnetic properties have highly skewed and wide distributions. Concentration-dependent magnetic properties (Table 1, grey-shading), such as χ, ARM, and $HIRM_{-300}$, are skewed to low values. The median χ value is $\sim 41 \times 10^{-8}$ m^3/kg, which is similar to topsoils from England and Wales ($\sim 37 \times 10^{-8}$ m^3/kg). Grain-size-dependent properties (Table 1, green-shading) are also skewed to low values; the median $\chi_{FD\%}$ value is about 6.5%, which suggests a significant fine-grained ferrimagnetic particle concentration. Coercivity-dependent properties (MDF_{ARM}, MDF_{IRM}, ARM_{EM2}, and IRM_{EM2}) and $HIRM_{AF100}$ (Table 1, blue-shading) are characterized by left-skewed distributions, while S-ratio, and the ARM_{EM1} proportions are skewed to higher values. This indicates that the remanent magnetization is dominated by soft magnetic components due to magnetite and maghemite.

3.3. Correlation of magnetic properties

Relationships among magnetic properties are often assessed to shed light on soil magnetic enhancement processes (Hu et al., 2013; Jordanova et al., 2016; Liu et al., 2010, 2013, 2015). Most magnetic parameters have non-Gaussian distributions and cannot be assumed to follow a linear relationship, so Spearman, rather than Pearson, correlation coefficients are calculated. Strong positive correlations are found among concentration-based parameters (Table 3, grey-shading). Correlations among grain size parameters are less strong. Coercivity and imperfect antiferromagnetic parameters, MDF_{IRM} and $HIRM_{AF100}$, correlate significantly. These parameters are best represented by magnetic minerals with B_{cr} larger than 100 mT. As expected, ARM and IRM EM properties correlate strongly with MDF_{ARM} and MDF_{IRM}, which suggests

Table 3
Spearman correlation coefficients for magnetic properties (471 samples).

	χ_{FD}	ARM	SIRM	$SIRM_{AF100}$	$HIRM_{-300}$	$\chi_{FD\%}$	ARM/SIRM	χ_{ARM}/χ	SIRM/χ	$HIMR_{AF100}$	S-ratio	MDF_{ARM}	MDF_{IRM}	IRM_{EM1}	IRM_{EM2}	ARM_{EM1}	ARM_{EM2}
χ	0.899	0.937	0.930	0.764	0.721	0.214	0.225		-0.179	-0.593	0.347	-0.258	-0.502	0.412	-0.412	0.403	-0.403
χ_{FD}		0.922	0.811	0.621	0.596	0.550	0.440	0.260	-0.243	-0.591	0.364	-0.303	-0.520	0.509	-0.509	0.498	-0.498
ARM			0.893	0.723	0.701	0.357	0.412	0.341	-0.130	-0.589	0.308	-0.319	-0.539	0.512	-0.512	0.505	-0.505
SIRM				0.886	0.818				0.140	-0.520	0.279	-0.172	-0.443	0.331	-0.331	0.325	-0.325
$SIRM_{AF100}$					0.932		-0.153		0.290								
$HIRM_{-300}$									0.248		-0.190	-0.143	-0.181	0.268	-0.268	0.273	-0.273
$\chi_{FD\%}$							0.681	0.545	-0.344	-0.286	0.226	-0.238	-0.279	0.415	-0.415	0.401	-0.401
ARM/SIRM								0.619	-0.628	-0.292		-0.393	-0.349	0.533	-0.533	0.527	-0.527
χ_{ARM}/χ												-0.243	-0.230	0.414	-0.414	0.419	-0.419
SIRM/χ										0.213	-0.172	0.222	0.181	-0.222	0.222	-0.212	0.212
$HIRM_{AF100}$											-0.678	0.351	0.785	-0.471	0.471	-0.456	0.456
S-ratio												0.164	-0.271				
MDF_{ARM}													0.689	-0.887	0.887	-0.895	0.895
MDF_{IRM}													-0.739		0.739	-0.740	0.740
IRM_{EM1}																0.997	-0.997
IRM_{EM2}																-0.997	0.997

Only values with correlations significant at the 0.01 level are shown.

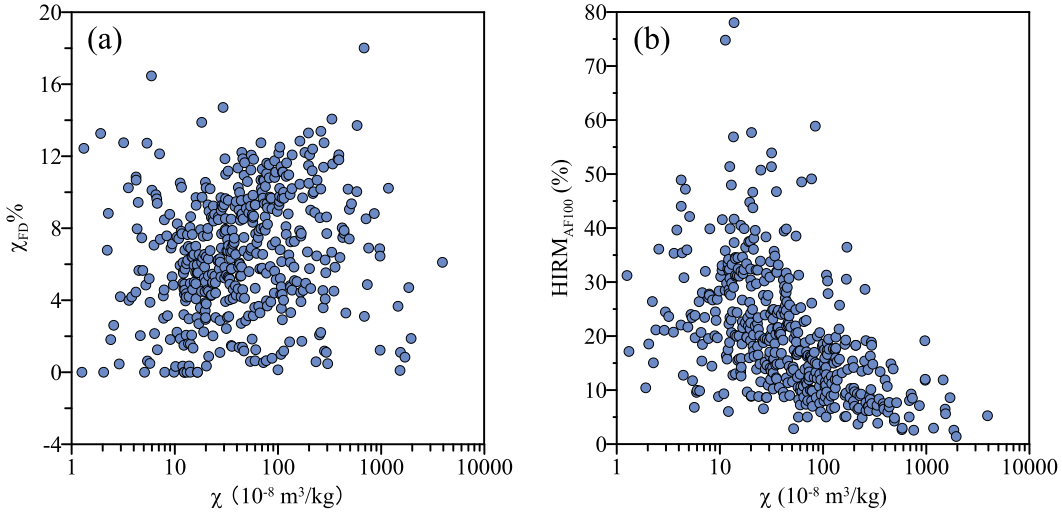

Fig. 3. Scatter plot of χ and (a) $\chi_{FD\%}$ and (b) $HIRM_{AF100}$.

that they represent the general coercivity distribution of the soil samples.

The most common magnetic enhancement mechanism in soils is via pedogenic fine magnetic particle production around the SP/SD boundary, as demonstrated by positive correlation between χ, χ_{fd}%, and pedogenic hematite signals (Hu et al., 2013; Liu et al., 2013; Torrent et al., 2006, 2007). However, no significant correlation is found for χ and χ_{fd}% for Australian soils (Fig. 3a), which indicates a minor pedogenic fine magnetic mineral contribution. Instead, $HIRM_{AF100}$ decreases with increasing χ (Fig. 3b), which suggests that low coercivity, most likely coarser, particles are responsible for the strong magnetism.

3.4. Principal component analysis of magnetic data

Dependencies exist among the studied magnetic properties, so PCA was carried out to find a low-rank approximation of the dataset. Four principal components (PC) can be used to elucidate ~80% of the variance; PC loadings for parameters are listed in Table 4. The main contributions to the first PC, which explain 35% of the variance, are MDF_{ARM} and the ARM and IRM EMs. Specifically, magnetically soft components have positive contributions, while hard components have negative contributions to PC1. The second PC explains 24% of the

Table 4
Eigenvalues and explained variance for the 4 leading principal components.

		PC1	PC2	PC3	PC4
	Latent	6.305	4.256	2.242	1.540
	Explained [%]	35.026	23.644	12.458	8.555
	Cumulative Contribution [%]	35.026	58.670	71.128	79.683
1	χ (10^{-8} m^3/kg)	0.172	**0.407**	0.059	0.054
2	χ_{FD} (10^{-8} m^3/kg)	0.200	0.306	0.165	**0.250**
3	ARM (10^{-6} Am^2/kg)	0.193	**0.364**	0.096	0.217
4	SIRM (10^{-4} Am^2/kg)	0.136	**0.402**	-0.035	-0.045
5	$SIRM_{AF100}$ (10^{-4} Am^2/kg)	0.103	**0.396**	-0.190	-0.024
6	$HIRM_{-300}$ (10^{-4} Am^2/kg)	0.110	**0.335**	-0.276	-0.052
7	$\chi_{FD\%}$	0.184	-0.128	0.221	**0.384**
8	ARM/SIRM (10^{-3})	0.204	-0.163	0.164	**0.446**
9	$\chi ARM/\chi$	0.145	-0.141	-0.038	**0.465**
10	SIRM/χ (10^3 A/m)	-0.131	0.110	-0.222	-0.088
11	$HIRM_{AF100}$ (%)	-0.245	-0.031	**-0.382**	0.266
12	S-ratio	0.057	0.062	**0.555**	-0.228
13	MDF_{ARM} (mT)	**-0.327**	0.149	0.183	0.200
14	MDF_{IRM} (mT)	-0.190	0.036	**-0.352**	**0.351**
15	ARM_{EM1}	**0.364**	-0.137	-0.169	-0.079
16	ARM_{EM2}	**-0.364**	0.137	0.169	0.079
17	IRM_{EM1}	**0.365**	-0.133	-0.151	-0.081
18	IRM_{EM2}	**-0.365**	0.133	0.151	0.081

Bold fonts represent parameters with the highest loadings in each PC.

variance and is governed by concentration-based magnetic parameters, including χ, ARM, and SIRM, which represent ferrimagnetic mineral concentration, and $SIRM_{AF100}$ and $HIRM_{-300}$, which are due to imperfect antiferromagnetic minerals. By comparison, χ_{FD} is less important in concentration-dependent parameters, which indicates that the superfine magnetic particle concentration around the SP/SD boundary is not the main contributor to the second factor. The third PC explains 12% of variance, with a major contribution from the relative importance of soft and hard magnetic components represented by $HIRM_{AF100}$, S-ratio, and MDF_{IRM}. S-ratio has the highest loading, which indicates that the proportion of soft magnetic components has the largest influence. The fourth PC explains 8% of variance and is dominated by magnetic grain size parameters ($\chi_{FD\%}$, ARM/SIRM, and χ_{ARM}/χ) that represent fine SP and SD ferrimagnetic particles, which all contribute positively to the fourth factor.

3.5. Magnetic parameter mapping

3.5.1. Variograms

Four magnetic properties, χ, ARM_{EM1}, S-ratio, and $\chi_{FD\%}$ were selected for mapping based on the presented PCA. For the fourth PCA, we choose $\chi_{FD\%}$ rather than χ_{ARM}/χ or ARM/SIRM. This choice was made because, compared to remanence-based parameters, changes in mineralogy have a weak influence on $\chi_{FD\%}$. Therefore, $\chi_{FD\%}$ is employed as a magnetic grain size indicator. First, outlier analysis was preformed quantitatively with Cooks method and then removed for each parameter. Removed outliers for each parameter and their geographical location are listed in Table S3. χ can be transformed to a nearly normal distribution by log10 transformation; no transformation is needed for $\chi_{FD\%}$; the S-ratio is transformed by a 5-degree power function transformation, and ARM_{EM1} is transformed by a cubic function. The histograms after transformation of these four parameters are shown in Fig. S3. Variograms and their fitting parameters are shown in Fig. 4. Spherical models give the best fit with a nugget effect for χ, $\chi_{FD\%}$, and ARM_{EM1}, and an exponential model with a nugget effect for S-ratio.

3.5.2. Continental contrasts in surface soil magnetic properties

Spatial patterns of concentration-dependent magnetic parameters are shown in maps in Fig. 5a. Systematic trends are not evident; however, several areas have strong magnetism: the Pilbara Province in the western plateau, including the Hamersley Range, Chichester Range, Augustus Range, and Nullagine Hills; the Nullarbor Plain in southwestern Australia, the Great Dividing Range in the eastern highlands, the Gulfs Ranges in South Australia, the Hervey Tablelands and Cairns Ranges in Queensland, and the Ord-Victoria Plateaus in northern Australia. In contrast, the Yaringa sandplain, Avon Plateau, Central lowlands, Murray lowlands, Carpentaria lowlands, and Barkly-Tanami Plains have the lowest magnetic mineral concentrations. Overall, high magnetic mineral concentrations, including ferrimagnetic minerals and hematite and goethite are mostly found in plateau and mountain areas, while lowlands and plains usually have weaker magnetism.

A map of the grain-size-dependent magnetic parameter $\chi_{FD\%}$ is presented in Fig. 5b. *Maxima* occur in the central Australian ranges, Yilgarn Plateau (sandplains), Nullarbor Plain, Murray lowlands (eolian

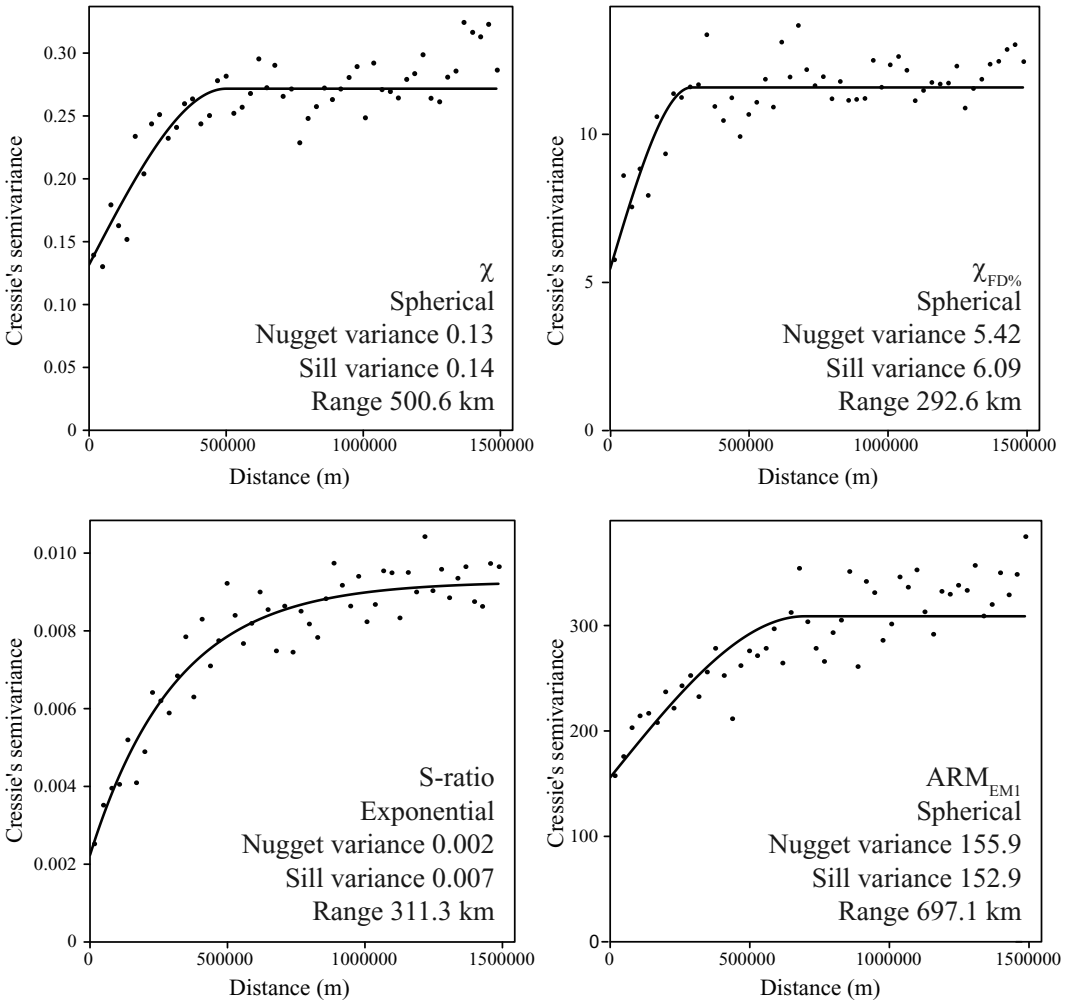

Fig. 4. Experimental variograms (dots) and fitted models (solid line) for magnetic parameters.

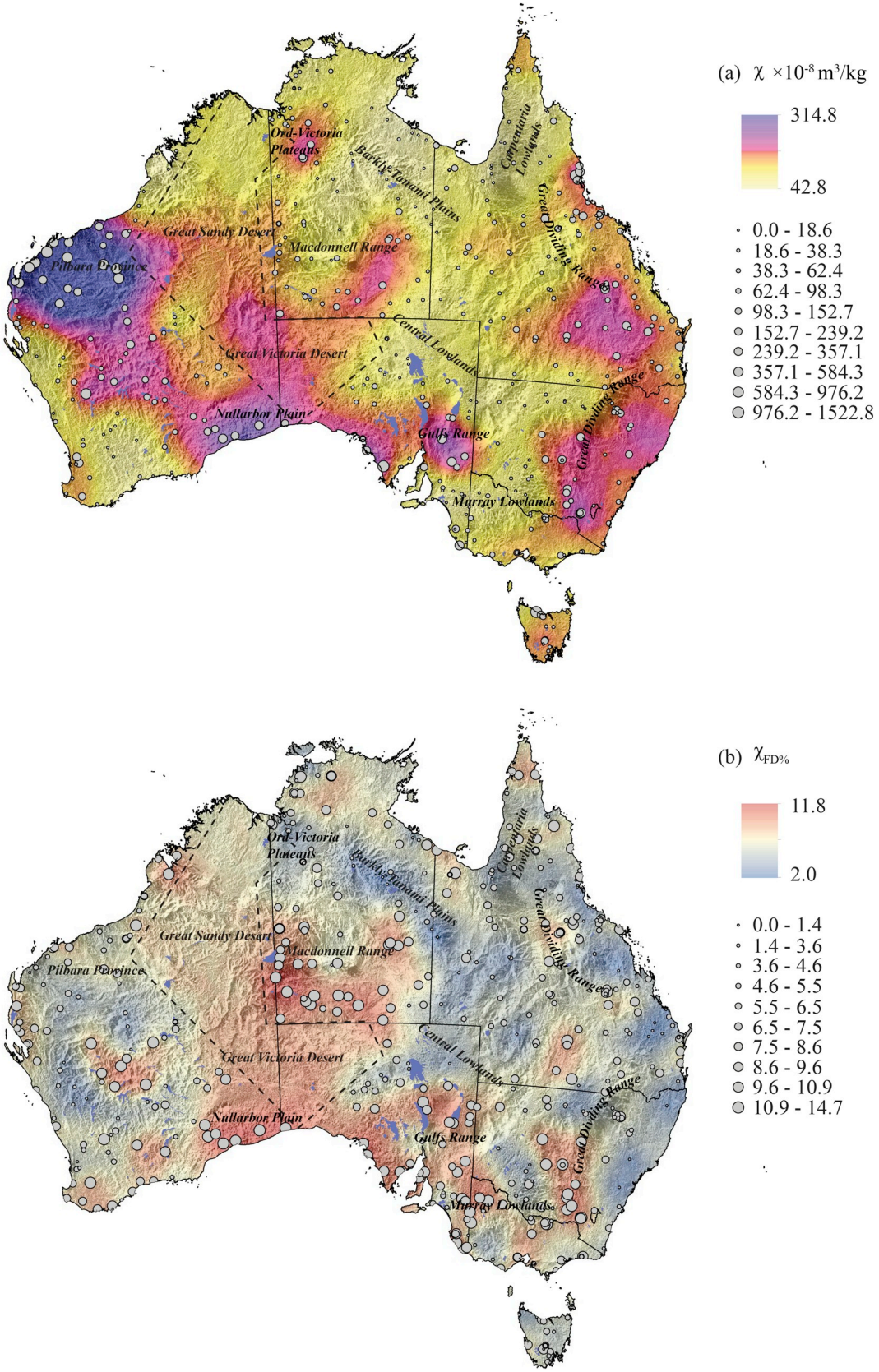

Fig. 5. Interpolated continental-scale maps of the spatial distribution of (a) χ and (b) $\chi_{FD\%}$ in Australia. The area within the black dashed lines was not sampled.

and alluvial sandplains, calcareous dunes), and Lake-Eyre plains, which are characterized by low ranges and tablelands with dunefields and sand plains. Lower values are found on the Barkly-Tanami Plain and Carpentaria lowlands in northern Australia, the Central Lowlands, Tasmania, eastern highlands and the Augustus Ranges in the western Plateau.

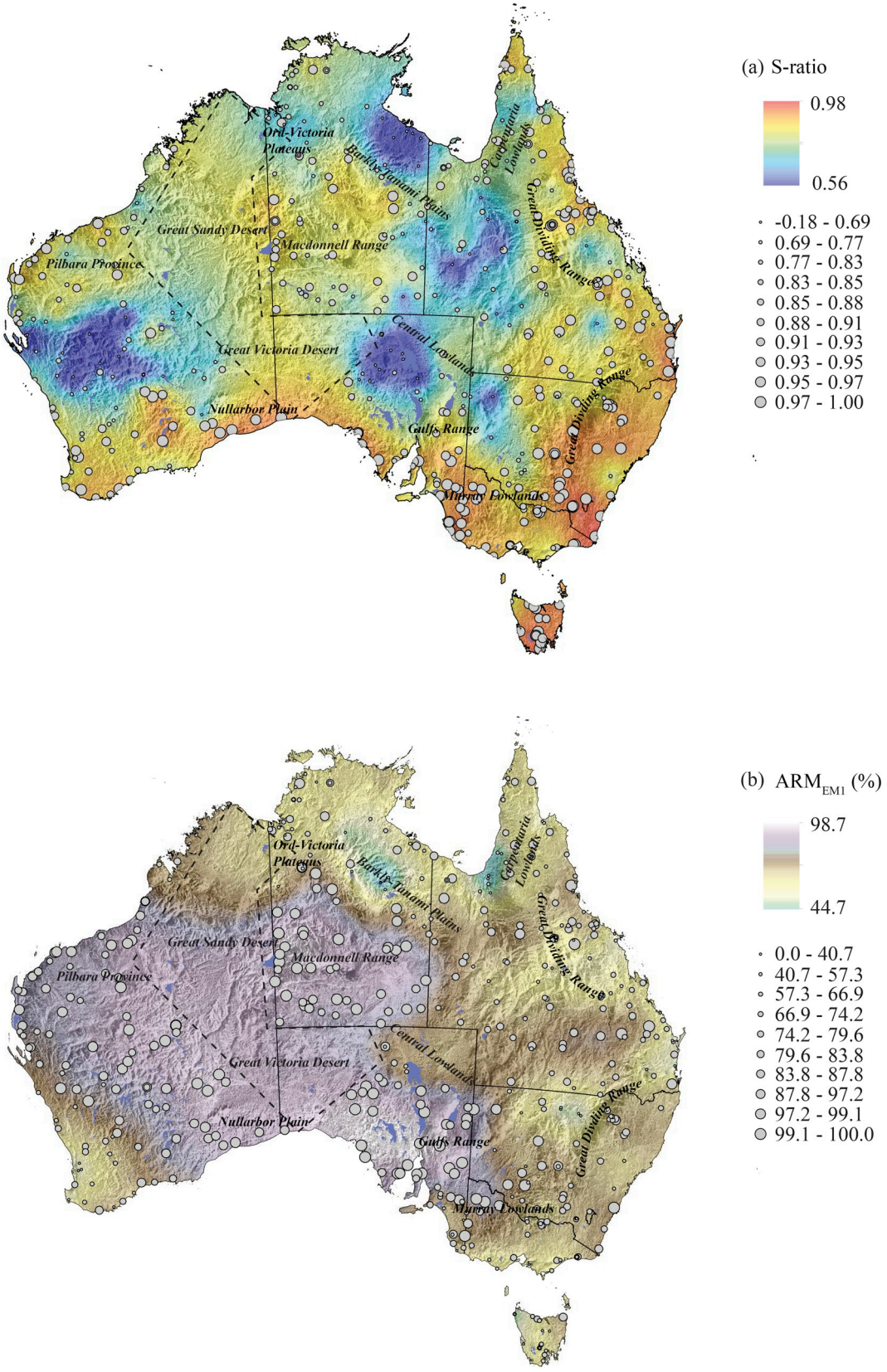

Fig. 6. Interpolated continental-scale maps of the spatial distribution of (a) S-ratio and (b) ARM_{EM1} in Australia. The area within the black dashed lines was not sampled.

The spatial distribution of the relative contribution of hematite and goethite to magnetite and maghemite (S-ratio) is shown in Fig. 6a. As expected, the vast central Australian interior, which is often referred to as the 'Red Centre', has significant hematite and goethite contributions, while in the southern Great Dividing Ranges, Nullarbor Plain, and Tasmania, their contribution to bulk magnetic properties is more limited.

Table 5
Ranked parent materials, land use, and age categories, based on median magnetic parameter values for associated soil samples.

Parent material	Count	χ (10^{-8} m^3/kg)		$\chi_{FD\%}$		S-ratio		ARM_{EM1}
Lacustrine sediments	13	19.90	Alluvium	5.60	Lacustrine sediments	0.80	Mafic volcanic rocks	68.27
Dunes	48	24.94	Mafic volcanic rocks	5.74	Alluvium	0.85	Alluvium	73.81
Sands	74	31.19	Ferruginous duricrusts	6.54	Dunes	0.86	Lacustrine sediments	75.42
Alluvium	228	35.50	Colluvium	6.84	Calcretes	0.87	Ferruginous duricrusts	79.45
Colluvium	20	45.55	Lacustrine sediments	6.99	Colluvium	0.88	Colluvium	80.42
Calcrete	14	67.71	Dunes	7.38	Igneous intrusive rocks	0.92	Sandstone/ mudstone	81.10
Igneous intrusive rocks	25	72.25	Sands	7.81	Sands	0.93	Igneous intrusive rocks	81.55
Sandstone/mudstone	15	77.35	Igneous intrusive rocks	8.50	Mafic volcanic rocks	0.93	Sands	82.66
Ferruginous duricrusts	17	121.22	Sandstone/mudstone	8.63	Sandstone/mudstone	0.94	Dunes	90.26
Mafic volcanic rocks	11	168.03	Calcretes	9.85	Ferruginous duricrusts	0.96	Limestone	91.40
Limestone	6	205.88	Limestone	11.50	Limestone	0.96	Calcretes	95.73

Land use	Count	χ (10^{-8} m^3/kg)		$\chi_{FD\%}$		S-ratio		ARM_{EM1}
NC	38	22.00	UI	3.93	GNV	0.84	NC	65.70
UI	8	26.47	RR	5.33	OPA	0.86	RR	67.97
OPA	34	33.07	GMP	5.61	UI	0.87	IC	69.10
IC	8	40.19	GNV	6.10	MU	0.91	GMP	72.93
GNV	254	41.94	IC	6.50	NC	0.92	PF	74.78
DC	36	42.19	MU	6.92	DC	0.93	DC	75.17
MU	38	44.83	DC	7.56	GMP	0.93	MU	75.28
GMP	41	45.26	NC	7.69	RR	0.94	UI	77.73
RR	6	54.09	OPA	8.21	IC	0.94	GNV	82.51
PF	8	131.87	PF	9.27	PF	0.97	OPA	90.00

Age	Count	χ (10^{-8} m^3/kg)		$\chi_{FD\%}$		S-ratio		ARM_{EM1}
Quaternary	307	35.28	Proterozoic	5.03	Quaternary	0.86	Paleozoic	77.76
Cenozoic	102	49.81	Quaternary	6.31	Proterozoic	0.90	Quaternary	78.64
Proterozoic	15	69.55	Paleozoic	6.54	Cenozoic	0.91	Mesozoic	81.32
Mesozoic	18	77.83	Mesozoic	6.57	Paleozoic	0.94	Cenozoic	81.61
Paleozoic	29	106.25	Cenozoic	7.43	Mesozoic	0.94	Proterozoic	86.99

NC, nature conservation; MU, other minimal use; IC, irrigated cropping; OPA, other protected area; GNV, grazing native vegetation; PF, production forestry; GMP, grazing modified pastures; DC, dryland cropping; UI, urban intensive uses; RR, rural residential and farm infrastructure.

The spatial distribution of the soft magnetic contribution (ARM_{EM1}) is shown in Fig. 6b. Generally, Western Australia, the central Australian ranges, and Eyre Peninsula have a larger proportion of low-coercivity magnetic components, which likely include both coarse (MD) and fine (just above the SP/SD boundary) ferrimagnetic minerals. Lower values in the east and north of Australia suggest a greater contribution of the hard magnetic component (EM2) in these areas.

3.6. Soil forming factors and Australian surface soil magnetism

Although soil forming processes are complex, specific soil forming factors (Jenny, 1941) are used widely to provide an explanatory framework for the role of individual environmental factors on soil attributes, such as magnetic properties, where a soil attribute S is given by f (Cl, O, R, P, T), where Cl, O, R, P, and T represent climate, organisms/vegetation, relief, parent material, and time, respectively. Each factor is discussed below in relation to Australian soil magnetism.

3.6.1. Parent material

Parent material types for the studied soil samples are summarized into 11 main groups in Table 5. The lower rankings of χ consist of mainly superficial materials, such as lake and coastal sediments, dunes, sand, alluvium, and colluvium. Such surface materials cover vast areas of Australia and represent > 80% of our sample set, which explains the generally weak magnetism of Australian surface soils. Lake and coastal sediments, dunes, alluvium, and colluvium also have lower S-ratios, which emphasizes the importance of hematite and goethite in Australian surface soils, which gives the continent red and yellow tones (Viscarra Rossel et al., 2010). Limestone, mafic volcanic rocks, and ferruginous duricrusts occupy the top rankings, respectively, for χ and S-ratio. These parent materials are mainly distributed in eastern mountain areas, Tasmania, the Nullarbor Plain, and northwestern plateau (Fig. 7a; compare with Figs. 5a, 6a). However, ferruginous duricrust materials, mafic volcanic rocks, and alluvium have the lowest $\chi_{FD\%}$ values, which indicates a lack of superfine magnetic particles. Calcretes, limestone, and sandstone/mudstone have the highest $\chi_{FD\%}$ values, which represent abundant superfine magnetic grains. Calcretes and limestones are mainly distributed in South Australia and in inland central and Western Australia (Fig. 7a).

For low coercivity components, calcretes, limestones, and dunes also have high ranks due to the high proportion of superfine magnetic particles around or just above the SP/SD boundary. In contrast, mafic volcanic rocks, lake and coastal sediments, and alluvium occupy the bottom 3 ranks for ARM_{EM1}, which indicates that they have generally higher coercivity magnetic mineral assemblages. Alluvium, lake sediments, and mafic volcanic rocks are all distributed mainly in eastern Australia, while calcretes, limestones, and dunes are distributed mainly in Western Australia (Fig. 7b), which is also consistent with the west-east ARM_{EM1} difference (Fig. 6b).

Kruskal-Wallis test results indicate significant differences between median values of different parent materials for all four magnetic parameters, which suggests a significant influence of parent material on the magnetic properties of Australian surface soils (Table 6). Scatter plots of median χ values for each parent material category versus individual samples also indicate a strong association of parent material with magnetic mineral concentration (Fig. 8b). The consistent pattern between parent material and magnetic parameters demonstrates that parent material is the dominant factor for surface magnetism. From multiple Kruskal-Wallis test comparisons (Table 6), not all parent material types have significantly different magnetism. For χ, superficial

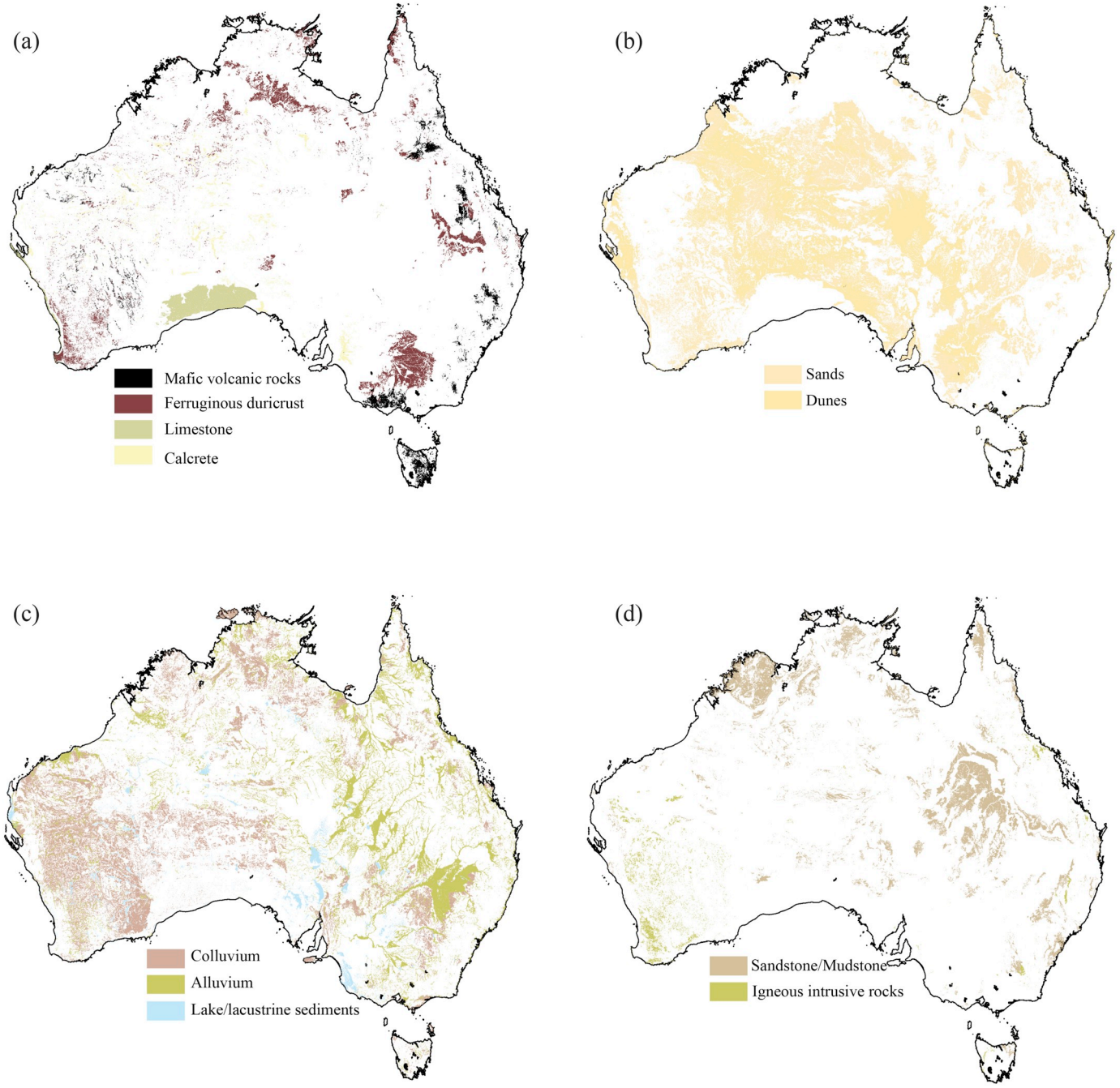

Fig. 7. Continental-scale spatial distribution of different parent material types.

desposits, such as alluvium, dunes, sands, and lake/coastal sediments have significantly ($p < .01$) lower values than iron-rich ferruginous duricrust materials and mafic volcanic rocks. For $\chi_{FD\%}$ and ARM_{EM1}, calcrete has the most distinctively high values compared to other materials. For S-ratio, alluvium and dunes have significantly low values, indicating a greater contribution from hematite and goethite.

3.6.2. Vegetation/land use

The studied samples fall into nine land use categories, including nature conservation (NC), other minimal use (MU), other protected area (OPA), grazing native vegetation (GNV), production forestry (PF), grazing modified pastures (GMP), dryland cropping (DC), urban intensive uses (UI), and rural residential and farm infrastructure (RR). GNV represents 54% of the data set and has relatively low rankings for χ, $\chi_{FD\%}$, and S-ratio (Table 5), which indicates low ferrimagnetic mineral concentrations but higher hematite and goethite contributions. RR and PF occupy the top rankings for both χ and S-ratio, but they only represent 3% of the total dataset. Samples with more anthropogenic influences, such as RR and UI have the lowest rankings on $\chi_{FD\%}$, which indicate that anthropogenic processes mainly produce coarser-grained magnetic minerals.

Unlike parent material, which has significant differences for all magnetic parameters, magnetic parameter differences with respect to land use categories are much weaker. Kruskal-Wallis test results (Table 6) indicate that land use categories are associated with no significant χ and $\chi_{FD\%}$ variation. S-ratio has the most significant variations among land use categories, which suggests that anthropogenic activities contribute most to the relative contribution of imperfect antiferromagnetic to ferrimagnetic minerals.

Table 6
Kruskal-Wallis test p values < .01 and multi-comparison results for categories of parent materials, land use types, and geological age.

Kruskal -Wallis	χ			$\chi_{FD\%}$			S-ratio			ARM_{EM1}		
	Overall	1.27E-06		Overall	4.93E-6		Overall	3.20E-12		Overall	4.95E-10	
Parent material	Mafic volcanic rocks	Alluvium	1.20E-02	Alluvium	Sands	5.19E-05	Alluvium	Sand	6.53E-07	Dunes	Alluvium	2.16E-06
		Dunes	5.30E-02		Calcrete	6.89E-03		Ferruginous duricrust	7.31E-04		Mafic volcanic rocks	1.10E-02
		Sands	1.30E-02					Mafic volcanic rocks	1.19E-02	Calcrete	Alluvium	2..05E-05
		Lacustrine sediments	8.00E-03					Igneous intrusive rocks	1.70E-03		Sands	1.36E-02
	Ferruginous duricrusts	Dunes	4.70E-02				Dunes	Sands	4.90E-03		Lacustrine sediments	1.05E-02
		Sands	1.20E-02					Ferruginous duricrusts	1.03E-02		Ferruginous duricrusts	3.10E-03
		Lacustrine sediments	1.20E-02					Igneous intrusive rocks	3.37E-02		Limestone	1.05E-02
											Mafic volcanic rocks	6.30E-04
Land use	Overall	> 0.01		Overall	> 0.01		Overall	5.03E-17		Overall	5.60E-5	
							DC	GNV	3.96E-06	NC	OPA	5.82E-04
								OPA	3.77E-02		GNV	1.45E-02
							GMP	GNV	9.35E-08	GMP	OPA	9.41E-04
								OPA	3.20E-03			
							GNV	MU	7.50E-03			
								NC	3.36E-04			
								PF	2.69E-04			
							OPA	PF	1.12E-02			
Age	Overall	> 0.01		Overall	> 0.01		Overall	1.62E-08		Overall	> 0.01	
							Quaternary	Cenozoic	1.52E-05			
								Paleozoic	9.92E-05			
								Mesozoic	3.46E-02			

NC, nature conservation; MU, other minimal use; OPA, other protected area; GNV, grazing native vegetation; PF, production forestry; GMP, grazing modified pastures; DC, dryland cropping; UI, urban intensive uses; RR, rural residential and farm infrastructure.

3.6.3. Geological time

Determining the time duration of pedogenesis is extremely difficult due to the combined effects of weathering, deposition, and erosion processes. During the last glacial period, many land masses were covered by ice sheets, which scraped away soil as they moved, which provides the main reference for determining pedogenic duration for European soils (Blundell et al., 2009a). However, during the last glaciation, ice was restricted to small upland areas in southeastern Australia, implying that Quaternary glaciation was not widely important for Australian soil formation. In addition to low erosion rates and long-lived tectonic stability, most Australian regolith has undergone deep weathering (Pain et al., 2012; Pillans, 2009). In places like the western cratonic shields, regolith formation can be traced to the Precambrian, but elsewhere it dates from the Paleozoic to the Holocene (Pillans, 2009) and it records superposed multiple weathering events under variable conditions. Therefore, we use the age of regolith or bedrock (if there is no surficial sediment) as the maximum weathering time.

The studied samples belong to 14 geological periods. However, considering the small sample numbers for some age periods, samples are organized into 5 groups (Quaternary, Cenozoic, Mesozoic, Paleozoic, and Proterozoic; Table 5). Quaternary samples have the lowest χ and S-ratio values, while Paleozoic and Mesozoic samples have higher values (Table 5). Based on the Kruskal-Wallis test (Table 6), only the S-ratio is significantly different for each age group. Quaternary

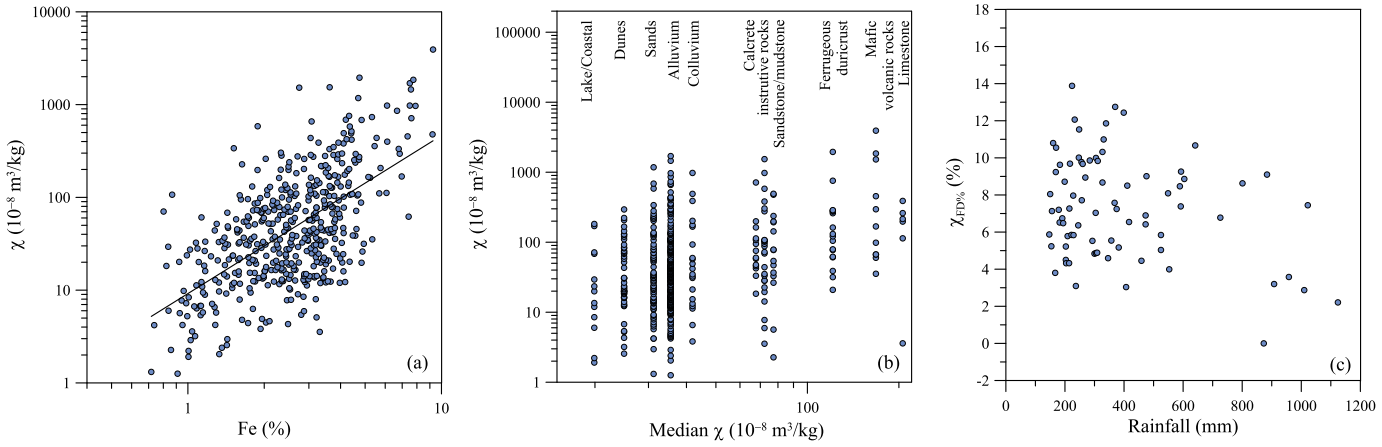

Fig. 8. Correlation between magnetic parameters and soil forming related factors. (a) Positive correlation between χ and Fe content; (b) scatterplot of median χ for each parent material category and individual sample values; and (c) relationship between rainfall and $\chi_{FD\%}$ for samples with clay contents < 20% and sand contents larger than 50%.

Table 7
Spearman correlation coefficients between variables for 471 samples.

	Relief/drainage			Climate		Organism/vegetation				Parent material	Age	Goethite, hematite	Major elements				
	Relief	Runoff	SHC	MAT	MAR	pH	OC	AW	Land use	Parent material	Age	NIODI	K	Fe	Si	Ca	Ti
χ		−0.117								0.247	0.156	−0.342	0.187	0.547	−0.401	0.364	0.400
$\chi_{FD\%}$			0.250	−0.130	−0.119			−0.197	0.199	0.271		−0.289					
S-ratio	0.295	0.307	0.155	−0.418	0.274	−0.149	0.455	−0.248	0.450	0.366	0.296	−0.191			−0.206	0.213	
ARM_{EM1}		−0.443	0.246		−0.497		−0.357		0.247	0.349		−0.441					−0.299
NIODI		0.244	−0.223		0.312			0.238	0.202	0.353							0.223

Only results with significant correlation at the $p < .01$ level are shown.

samples have low S-ratios and χ, which suggests that younger samples are generally weakly magnetic with a greater proportion of imperfect antiferromagnetic minerals.

4. Discussion

4.1. Influencing factors for Australian surface soil magnetism

Spearman correlation analysis was carried out for four magnetic parameters, 18 soil forming and soil property factors, including three relief and drainage factors, two climate factors, four organism/vegetation factors, time, NIODI ratio, and five major elements, to investigate the most influential factors for Australian surface soil magnetism. Results with correlation coefficients above the 0.01 significance level are shown in Table 7 and are discussed below.

4.1.1. Magnetic mineral concentration

Both Spearman correlation analysis and the Kruskal-Wallis test reveal the importance of parent material in explaining χ variability, which is representative of magnetic mineral concentration. Fe, Ca, and Ti concentration have the highest positive correlation with χ (Table 7, Fig. 8a). Ti is resistant to weathering and anthropogenic input of both Fe and Ti can be ignored because most samples were collected from protected areas or uncultivated fields. Therefore, the strong positive relationship of Fe and Ti with χ indicates that Fe derived from bedrock weathering, eolian transportation, or hydraulic regolith erosion is the dominant contributor to magnetic mineral concentration. Ca also has a strong positive correlation with χ (Table 7). For Australian soils, the main regional and national-scale controls on soil calcium carbonate distribution are driven by parent material and climate, specifically rainfall, temperature, and seasonality (Wilford et al., 2015). Consequently, high χ in carbonate-rich parent material (discussed later) is one reason of strong positive correlation between Ca and χ. Relatively low rainfall and high evapotranspiration, which are conducive to the accumulation and retention of calcium carbonate within the soil from either atmospheric sources and/or underlying bedrock (Wilford et al., 2015), also aids preservation of magnetic minerals from dissolution or leaching. Negative correlation of Si and χ can then be explained easily because paramagnetic and diamagnetic minerals, such as clay minerals and quartz will inevitably dilute magnetic assemblages. Ranking of χ for different parent materials (Table 5) indicates that samples from alluvium, dunes, sands, and lacustrine sediments lack magnetic minerals, while soils developed on mafic volcanic rocks, ferruginous duricrusts, and limestones have the strongest magnetism, which demonstrates that bedrock weathering is the main iron source and the reason for their strong magnetism. Mafic volcanic rocks, such as basalt, are rich in iron and primary magnetite or titanomagnetite. Soils derived from mafic volcanic units have enhanced χ due to the presence of magnetite/titanomagnetite that is weathered directly from the parent material, which explains the high χ values in these soils. Mafic rocks are distributed mainly in the eastern highlands and western plateau (Fig. 7a) such as, in the east, the Fitzroy Uplands, the New England-Moreton uplands, the Kosciuszkan uplands, the Tasmanian uplands, and, in the west, Hamersley Plateau, Murchison Plateau, and the Southern Goldfield Plateau. Magnetite mining accelerates physical weathering of iron-rich parent materials and is another possible source of coarse magnetite in the Pilbara and Western Australia.

An important feature of the Australian landscape is the widespread occurrence of ferruginous and siliceous duricrusts (Anand, 2005). Based on their origins, two major ferruginous duricrust types are recognized: lateritic residuum and ferricrete (Anand, 2001). Most ferruginous samples in this study come from lateritic residuum, which is commonly most strongly developed on iron-rich rocks (Anand, 2005). Lateritic residuum formation involves repeated in situ processes, such as iron oxide precipitation, continued clay dissolution, dehydration, nodule and pisolith development, collapse of mottled saprolite, and introduction of exotic materials through soil forming and eolian processes (Anand, 2001). Lateritic residuum is exposed as isolated hills or as meandering ridges due to relief inversion. Thin soils on such ferruginous duricrusts most likely inherited maghemite in the upper pisolitic part to produce high χ values.

Soils with limestone and calcrete parent material mainly occur in the Eucla Basin along the Great Australian Bight (Fig. 7a). The Eucla Basin is characterized by well-preserved paleovalley systems that extend toward the interior into surrounding Precambrian cratons (Hou et al., 2000; Otrakdjian and Keeling, 2010). The hinterland regions have extensive exposures that are considered primary sources, and sedimentary basins that act as traps for detritus from hinterland regions that are considered secondary sources (Johnson, 2015). U-Pb zircon analysis indicates that the most likely source regions are the Musgrave Provinces, Yilgarn Craton, Officer Basin, Albany-Fraser Orogen, and Gawler Craton (Johnson, 2015). Iron-rich rocks in these hinterlands would have been sources for magnetic grains that have typically spent millions of years being weathered. The Eucla paleo-drainage systems and wind will have transported them to the Eucla Basin and Nullarbor Plain, where they have been preserved due to the extremely dry climate. Meanwhile, rainwater dissolves $CaCO_3$ and transports it to the water table, leaving insoluble components (e.g., quartz, iron oxides, and clay minerals) concentrated in the upper part (Lowry, 1971), which results in sandy, red, and relatively strongly magnetic surface soils. Although calcrete forms authigenically, iron oxides are mainly residual derivatives of source region rocks that accumulate in indurated ferruginous duricrusts (Anand and Paine, 2002).

In summary, soils that form on igneous rocks can accumulate primary magnetic minerals from parent materials through surface weathering and accumulation of magnetite and maghemite, such as in the eastern uplands and in some high relief areas in the western plateau. For low relief areas, magnetic minerals are concentrated during ferruginization or by eolian and fluvial processes. Notably, areas with stronger magnetism are less weathered (Wilford, 2012): the eastern uplands and Hamersley Ranges, which also suggests a mainly lithogenic control. Therefore, consistent with previous studies of England and

Wales (Blundell et al., 2009b) and Bulgaria (Jordanova et al., 2016), parent material is the most important factor for surface soil magnetism because it provides an iron source and an erodible source of resistant magnetic minerals.

4.1.2. Magnetic mineral grain size

It is important to note that the concentration of superfine ferrimagnetic particles is also mostly influenced by parent material, where χ, χ_{FD}, ARM, SIRM, $HIRM_{AF100}$, and HIRM belong to the same PCA group. $\chi_{FD\%}$ mainly represents the ferrimagnetic mineral grain size distribution, which indicates the relative importance of superfine ferrimagnetic particles near the SP/SD boundary.

Rainfall is generally considered the most important factor for pedogenic superfine particle formation. Magnetic grain size parameters are used as paleoprecipitation proxies for Quaternary loess-paleosol systems (Geiss et al., 2008; Maher et al., 1994) because increased rainfall favours pedogenic SP and SD magnetic mineral production, which results in higher χ_{ARM}/IRM and χ_{ped} (the difference in the magnetic susceptibility between the soil B-horizon and the parent material) values. However, the positive relationship usually fails for rainfall > ~1000 mm/yr because iron oxide dissolution and leaching increases in water-saturated soils or where precipitation is < 200 mm/yr because of slow pedogenesis (Maher, 2011).

For UK and Bulgarian national surface soil surveys, no significant correlation has been reported between rainfall and magnetic properties (Blundell et al., 2009a; Jordanova et al., 2016). Blundell et al. (2009a) argued that the influence of rainfall on magnetic properties is complicated by parent material and drainage differences, while Jordanova et al. (2016) suggested that the major role of climate in pedogenic ferrimagnetic mineral enhancement is related to primary parent material weathering. However, both studies indicate that by constraining parent material, fine magnetic components have a positive relationship with rainfall, which reflects pedogenic soil enhancement. Australian surface soils have a weak negative relationship between rainfall and superfine ferrimagnetic particle contents (Table 7). Australia is arid with a low annual average rainfall of 419 mm, where 80% of Australia has rainfall of < 600 mm/yr and 50% has < 300 mm/yr. Therefore, the negative relationship with rainfall cannot be explained by dissolution in water-logged soils. Slow pedogenesis rates could explain the generally weak correlation between rainfall and superfine ferrimagnetic particles. Parent material also has a significant influence on fine ferrimagnetic minerals, which is consistent with previous studies in Europe. However, instead of a positive relationship, a weak negative relationship is found for Australian surficial soils. On the one hand, long weathering in hot, arid climates will cause progressive transformation of iron-bearing minerals to hematite. The weak magnetism of hematite and its widespread importance in Australian soils could, therefore, correlate negatively with rainfall, which is also supported by weak negative correlation between $\chi_{FD\%}$ and MAT. On the other hand, increasing rainfall could wash out or cause leaching of fine magnetic particles in surface soils. Most soil samples in this study developed on sandy substrates that lack iron. Therefore, rather than promoting pedogenic magnetic mineral formation, increasing rainfall could cause migration of fine magnetic minerals out of soils. This hypothesis is further demonstrated by Fig. 8c. By selecting sandy samples (< 20% clay and > 50% sand), a decreasing $\chi_{FD\%}$ trend is shown with increasing rainfall. This trend becomes clearer above 600 mm, which is potentially the rainfall threshold for significant washing or leaching.

$\chi_{FD\%}$ correlates positively with SHC, which suggests that the hydraulic conductivity has a significant influence on the formation and/or preservation of superfine magnetic particles. Hydraulic conductivity is correlated to soil properties, such as pore size and soil texture. Sandy soils usually have higher SHC, which prevent water-logging that may dissolve fine particles.

4.1.3. Coercivity distributions of magnetic minerals

The S-ratio represents the relative importance of ferrimagnetic minerals to hematite and goethite, while ARM_{EM1} represents the portion of 'soft' magnetic minerals with median coercivity of ~13 mT. Climate, organisms/vegetation, and parent material are the most important factors for S-ratio and ARM_{EM1} (Table 7). ARM_{EM1} correlates negatively with rainfall, possibly also due to leaching or erosion of fine magnetic particles. Parent material not only determines the magnetic mineral concentration by influencing iron supply; it also influences the relative magnetic mineral composition, which indicates that weathering does not change completely the mineral composition of bedrock or parent material.

Hematite and goethite formation and preservation reflect pH, moisture, and temperature conditions in the soil environment, which is why S-ratio correlates strongly with MAT and organic carbon (Table 7). Warmer climates favour oxidation of magnetite and maghemite to hematite and goethite. In the tropics, where MAT is higher, hematite and goethite can accumulate in large quantities in surficial environments with intense weathering to form ferricrete or ferruginous duricrusts (Aleva, 1994; Eggleton, 2001), which contributes to the negative correlation of S-ratio and MAT. Land use also influences strongly the relative importance of ferrimagnetic and imperfect antiferromagnetic minerals. Generally, greater agricultural and anthropogenic activity, such as production forestry, rural residential, and farm infrastructure, have the highest ferrimagnetic mineral portions, while land with natural vegetation has the highest hematite and goethite contents. Most airborne iron oxides have an anthropogenic origin in the form of aggregated magnetite nanoparticles (Moteki et al., 2017), which contributes to higher S-ratios in areas with intense anthropogenic activity. Production forests and rural residential and farm infrastructure occur mostly close to the largest cities, such as Sydney and Melbourne, which have localized influences. Most of the studied samples are from natural wild lands, which have lower S-ratios due to larger hematite and goethite contributions.

Organic carbon correlates positively with S-ratio but negatively with ARM_{EM1} (Table 7). This could indicate ferrimagnetic mineral dissolution in organic-rich environments and relative enrichment of higher coercivity minerals (e.g., Roberts, 2015). Such reactions are common in organic-rich podzolized soils. While organic carbon provides fuel for dissimilatory iron reducing bacteria that reduce Fe^{3+} to Fe^{2+}, with excess Fe^{2+} reacting with ferrihydrite to produce SP or SD magnetite (Blundell et al., 2009a), lack of magnetic enhancement in organic-rich soils indicates that this process is not widely active in the studied Australian soils.

4.1.4. The relative importance of hematite and goethite

Based on the above discussion, hematite and goethite concentrations and their relative contributions with respect to ferrimagnetic counterparts depend mainly on parent material, land use, organic carbon, and MAT. Environmental factors that influence the hematite/goethite ratio and the relationship between the hematite/goethite ratio and other magnetic properties is an important topic for soil iron oxide research (Balsam et al., 2004; Hao et al., 2009; Hu et al., 2016; Ji et al., 2004; Jordanova et al., 2011a; Lyons et al., 2014; Viscarra Rossel et al., 2010). Viscarra Rossel et al. (2010) published the first iron oxide maps of Australian surface soils, which reveal that soils with high hematite to goethite contents are prevalent in western and central Australia, while a large swath of soils across northern and eastern Australia, and the southwestern corner of Australia, are dominated by goethite. This distribution is as expected from the contrasting climate regimes in Australia. In oxic terrestrial environments, a range of initially formed ferric (oxy-) hydroxides such as goethite, limonite, and ferrihydrite dehydrate with time to form hematite (Berner, 1969). This reaction is favoured by the absence of water and elevated temperatures (Berner, 1969; Maher, 1986), so that hematite is an environmentally important iron oxide in arid environments (e.g., Larrasoaña et al., 2003), including those in

Parent Material	Distribution	Weathering	Iron oxides	Magnetic parameters
Iron rich bedrock	Hill belts, Mountain area, Plateau Eastern uplands, Tasmania and northwest of western plateau	Slightly - Moderately weathered	Primary minerals preserved magnetite titanomagnetite	High χ, ARM, SIRM; Low χ_{ARM}/χ, $\chi_{FD\%}$; High S-ratio
Ferrigunous duricrust	Dissected paleo-landsurface; isolated hills; meandering ridges due to relief inversion	Highly weathered	Accumulation of iron oxides by down-washing Maghemite, hematite, goethite	High χ, ARM, SIRM; Low χ_{ARM}/χ, $\chi_{FD\%}$; High S-ratio;
Calcrete Limestone	Semi-arid regions Nullarbor Plain	Lack of leaching low rainfall	Accumulation of iron oxides from eolian input or runoff Fine particles of maghemite, hematite, goethtie	High χ, ARM, SIRM; High χ_{ARM}/χ, $\chi_{FD\%}$; High ARM_{EM1}
Low iron superficial sediments	Widely distributed deserts, lowland	Eolian, alluvial, colluvial processes, dust events	Low concentration of iron oxides	Low χ, ARM, SIRM; Variable other magnetic parameters

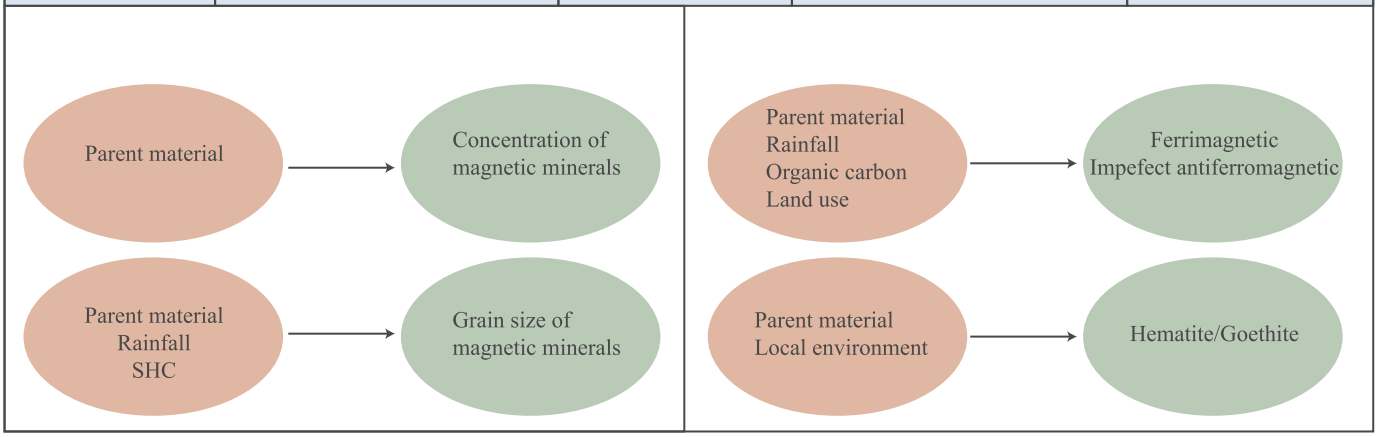

Fig. 9. Proposed mechanisms that control the magnetic properties of Australian surface soils.

western and central Australia. In wetter continental environments, goethite is more likely to persist, as is the case across northern, eastern, and southwestern Australia. This distribution pattern is also consistent with the positive correlation between NIODI and MAR (Table 7), where high temperatures favour hematite while high rainfall favours goethite, as suggested by previous studies (Balsam et al., 2004; Cornell and Schwertmann, 2004; Ji et al., 2004; Viscarra Rossel et al., 2010). The S-ratio distribution is similar to the ARM_{EM1} map (Fig. 6a, b), where ARM_{EM1} correlates negatively with the NIODI ratio derived from Viscarra Rossel et al. (2010), which indicates that the hematite content is related closely to the soft magnetic particle content.

Singh and Gilkes (1992) studied hematite and goethite in southwestern Australian soils and found that both minerals are highly aluminium substituted (13–35 mol% for goethite and 4–23% mol% for hematite, respectively). Increasing aluminium substitution results in decreasing hematite and goethite grain size (Jiang et al., 2012, 2014), so that pedogenic hematite and goethite in Australian soils must be extremely fine-grained. According to Singh and Gilkes (1992), the average mean crystal dimension of their soil goethite and hematite is ~20 nm and ~15 nm, respectively. Hematite and goethite in this size range will be close to the SP/SD threshold size, with low coercivity (Banerjee, 1971; Hu et al., 2016; Jiang et al., 2012, 2014). Therefore, negative correlation between the NIODI ratio and $\chi_{FD}\%$ and ARM_{EM1} indicates that most Australian surface soil hematite is nanosized with low coercivity, and will contribute to $\chi_{FD\%}$ and ARM_{EM1} with other ferrimagnetic minerals. Such pigmentary hematite also contributes red colours to the Australian landscape.

At the continental scale, the NIODI ratio correlates weakly with other soil, climate, and geographic factors, possibly due to the relatively small number of samples and the dominant effect of local micro-environments. Viscarra Rossel et al. (2010) pointed out that hematite is often associated with kaolinitic and illitic clays, while smectitic soils are associated with goethite. Ferruginization and silicification are the most important landscape processes in Australia and also for hematite and goethite accumulation. According to Anand (2005), free drainage and a high Fe precipitation temperature in duricrusts gives rise to hematite formation, while low precipitation temperature, moist conditions, and abundant organic matter produce goethite (Anand, 2005). From our results, parent material and available soil water content have a relatively stronger relationship with the NIODI ratio, which also suggests a lithogenic control and local variation due to vegetation/organisms.

4.2. Conceptual model for Australian surface soil magnetism

We identify a dominant influence of parent material/iron source on Australian surface soil magnetism. Climate, drainage, and organisms are further important elements. Factors such as temperature, organic carbon, and land use only have a strong influence on the S-ratio, which indicates that hematite and goethite formation/preservation involves multiple complex processes, including physical and chemical weathering, ferruginization, and biochemical effects. We propose the following conceptual model based on our results (Fig. 9).

Iron-rich bedrock such as basalt, which is distributed on mountain areas and plateaus, usually experiences low to moderate weathering

due to relatively low erosion rates (Anand, 2005; Wilford, 2012). Weathering products are primary minerals, where iron oxides in these thin soils are mainly coarse magnetite and/or titanomagnetite that eroded from mafic/ultramafic bedrock to produce high χ and S-ratios, and low $\chi_{FD\%}$ values. Ferruginous duricrusts are distributed mainly in dissected paleo-landscape surfaces with low to moderate relief, isolated hills, and meandering ridges due to relief inversion. After prolonged strong weathering, iron oxides accumulate by down-washing of soluble components. High χ, S-ratio, and ARM_{EM1} values, and low $\chi_{FD\%}$ values of soils that developed on ferruginous duricrusts indicate that they mainly inherited coarse maghemite from ferruginous duricrusts. Soils that developed on volcanic rocks and ferrigunious duricrusts have similar magnetic properties, which suggest a dominant lithogenic control for soils developed on iron-rich materials.

Calcretes occur mainly in arid or semi-arid regions. Studied samples that formed on calcretes are mostly from the Nullarbor Plain and Eucla Basin. Under arid conditions, fine magnetic particles accumulated due to eolian inputs or rock runoff to produce high χ, $\chi_{FD\%}$, and ARM_{EM1} values.

Surficial sediments are distributed widely in deserts and vast inland areas of Australia. These materials generally lack iron, and accumulate minor magnetic minerals from eolian, alluvial, and colluvial processes, to produce weak magnetism. Soils developed on these sediments have variable magnetic properties due to their complex origin and pedogenic processes.

Soil forming factors influence Australian surface soil magnetic properties in different ways (Fig. 9). Parent material provides the main iron source that controls both ferrimagnetic and imperfect antiferromagnetic mineral concentrations, grain size distribution, and relative contribution of hematite to goethite. Soil texture affects fine magnetic particles in two ways: higher hydraulic conductivity prevents waterlogging and washing away of fine particles from sandy soils with intense rainfall. Multiple factors, including parent material, temperature, organic carbon, and land use, influence the relative importance of ferrimagnetic and imperfect antiferromagnetic minerals, which integrate lithogenic and pedogenic processes.

5. Conclusions

We present a comprehensive magnetic property analysis of surficial soils across Australia, with maps of selected magnetic properties representing magnetic mineral concentration, grain size, the relative importance of ferrimagnetic minerals to imperfect antiferromagnetic minerals, and low coercivity contributions to illustrate spatial patterns in Australian soil magnetic properties. Observed magnetic property ranges suggest a large variation of magnetic minerals and their concentrations in surficial soils. The main pattern in Australian surface soils is of low magnetic mineral concentrations. Principal component analysis reveals that the coercivity and concentration of ferrimagnetic minerals provide > 50% of the total variance in the magnetic properties of Australian surface soils. Maps are presented for four major magnetic properties. The vast continental interior of Australia is characterized by low ferrimagnetic mineral concentrations, with higher hematite and goethite contributions. Hotspots with strong magnetism are found on the northwestern plateau, Eucla Basin, and eastern highlands.

The influence of soil forming factors on Australian surface soil magnetic properties is evaluated systematically and a conceptual model is proposed to explain magnetic mineral processes in Australian soils. Parent material is the dominant factor that controls magnetic properties by providing iron sources and releasing magnetic minerals by weathering. Temperature, organic carbon content, and land use affect hematite and goethite formation and preservation at local scales. The relative importance of hematite and goethite is more complicated for all factors, where parent material and local vegetation/organic conditions have relatively stronger influences.

Supplementary data to this article can be found online at https://doi.org/10.1016/j.earscirev.2019.103028.

Declaration of Competing Interest

The authors declare that they have no known competing financial interests or personal relationships that could have appeared to influence the work reported in this paper.

Acknowledgements

This work was supported by the Australian Research Council through grants DP160100805 and DP190100874. We thank Prof. Qingsong Liu for helpful discussion, Dr. Chuan Lu for help with data processing, Dr. Patrice de Caritat for mapping suggestions, and four anonymous reviewers whose comments improved this paper. The data presented here can be found in the PANGAEA database portal (http://www.pangaea.de).

References

Ahmed, I.A.M., Maher, B.A., 2018. Identification and paleoclimatic significance of magnetite nanoparticles in soils. Proc. Natl. Acad. Sci. U. S. A. 115 (8), 1736–1741.
Aleva, G.J.J., 1994. Laterites: Concepts, Geology, Morphology and Chemistry. Wageningen, International Soil Reference and Information Centre (169 pp).
Anand, R.R., 2001. Evolution, classification and use of ferruginous regolith materials in gold exploration, Yilgarn Craton, Western Australia. Geochem. Explor. Environ. Anal. 1 (3), 221–236.
Anand, R.R., 2005. Weathering history, landscape evolution and implications for exploration. In: Butt, C.R.M., Robertson, I.D.M., Scott, K.M., Cornelius, M. (Eds.), Regolith Expression of Australian Ore Systems: A Compilation of Exploration Case Histories with Conceptual Disperson, Process and Exploration Models. CRC LEME, Perth, W.A, pp. 15–45.
Anand, R.R., Paine, M., 2002. Regolith geology of the Yilgarn Craton, Western Australia: implications for exploration. Aust. J. Earth Sci. 49, 4–162.
Ashton, L.J., McKenzie, N.J., 2001. Conversion of the Atlas of Australian Soils to the Australian Soil Classification. CSIRO Land and Water. https://data.gov.au/data/dataset/9b3cbd51-d403-4dd1-bc88-3bb3d97eb322.
Ayoubi, S., Karami, M., 2019. Pedotransfer functions for predicting heavy metals in natural soils using magnetic measures and soil properties. J. Geochem. Explor. 197, 212–219.
Ayoubi, S., Ahmadi, M., Abdi, M.R., Abbaszadeh Afshar, F., 2012. Relationships of ^{137}Cs inventory with magnetic measures of calcareous soils of hilly region in Iran. J. Environ. Radioact. 112, 45–51.
Ayoubi, S., Soltani, Z., Khademi, H., 2018. Particle size distribution of heavy metals and magnetic susceptibility in an industrial site. Bull. Environ. Contam. Toxicol. 100 (5), 708–714.
Ballabio, C., Panagos, P., Monatanarella, L., 2016. Mapping topsoil physical properties at European scale using the LUCAS database. Geoderma 261, 110–123.
Balsam, W., Ji, J., Chen, J., 2004. Climatic interpretation of the Luochuan and Lingtai loess sections, China, based on changing iron oxide mineralogy and magnetic susceptibility. Earth Planet. Sci. Lett. 223 (3), 335–348.
Balsam, W.L., Ellwood, B.B., Ji, J., Williams, E.R., Long, X., El Hassani, A., 2011. Magnetic susceptibility as a proxy for rainfall: worldwide data from tropical and temperate climate. Quat. Sci. Rev. 30 (19), 2732–2744.
Banerjee, S.K., 1971. New grain size limits for palaeomagnetic stability in haematite. Nat. Phys. Sci. 232, 15–16.
Barrón, V., Torrent, J., de Grave, E., 2003. Hydromaghemite, an intermediate in the hydrothermal transformation of 2-line ferrihydrite into hematite. Am. Mineral. 88 (11 – 12), 1679–1688.
Batjes, N.H., 2016. Harmonized soil property values for broad-scale modelling (WISE30sec) with estimates of global soil carbon stocks. Geoderma 269, 61–68.
Berner, R.A., 1969. Goethite stability and the origin of red beds. Geochim. Cosmochim. Acta 33 (2), 267–273.
Bloemendal, J., Lamb, B., King, J., 1988. Paleoenvironmental implications of rock-magnetic properties of late Quaternary sediment cores from the eastern equatorial Atlantic. Paleoceanography 3 (1), 61–87.
Blundell, A., Dearing, J.A., Boyle, J.F., Hannam, J.A., 2009a. Controlling factors for the spatial variability of soil magnetic susceptibility across England and Wales. Earth Sci. Rev. 95 (3–4), 158–188.
Blundell, A., Hannam, J.A., Dearing, J.A., Boyle, J.F., 2009b. Detecting atmospheric pollution in surface soils using magnetic measurements: a reappraisal using an England and Wales database. Environ. Pollut. 157 (10), 2878–2890.
Brevik, E.C., Calzolari, C., Miller, B.A., Pereira, P., Kabala, C., Baumgarten, A., Jordán, A., 2016. Soil mapping, classification, and pedologic modeling: history and future directions. Geoderma 264, 256–274.
Butler, R.F., Banerjee, S.K., 1975. Theoretical single-domain grain-size range in magnetite and titanomagnetite. J. Geophys. Res. 80 (29), 4049–4058.
Carcaillet, C., Richard, P.J.H., Asnong, H., Capece, L., Bergeron, Y., 2006. Fire and soil

erosion history in East Canadian boreal and temperate forests. Quat. Sci. Rev. 25 (13), 1489–1500.
Chaney, N.W., Wood, E.F., McBratney, A.B., Hempel, J.W., Nauman, T.W., Brungard, C.W., Odgers, N.P., 2016. POLARIS: a 30-meter probabilistic soil series map of the contiguous United States. Geoderma 274, 54–67.
Chaparro, M.A.E., Gogorza, C.S.G., Chaparro, M.A.E., Irurzun, M.A., Sinito, A.M., 2006. Review of magnetism and heavy metal pollution studies of various environments in Argentina. Earth Planets Space 58 (10), 1411–1422.
Colombo, C., Palumbo, G., He, J.Z., Pinton, R., Cesco, S., 2014. Review on iron availability in soil: interaction of Fe minerals, plants, and microbes. J. Soils Sediments 14 (3), 538–548.
Cook, R.D., 1977. Detection of influential observation in linear regression. Technometrics 19 (1), 15–18.
Cook, R.D., 1979. Influential observations in linear regression. J. Am. Stat. Assoc. 74 (365), 169–174.
Cornell, R.M., Schwertmann, U., 2004. The Iron Oxides: Structure, Properties, Reactions, Occurences and Uses. Wiley-VCH Verlag GmbH & Co, KGaA (664 pp).
Crockford, R.H., Fleming, P.M., 1998. Environmental magnetism as a stream sediment tracer: an interpretation of the methodology and some case studies. Soil Res. 36 (1), 167–184.
Crockford, R.H., Olley, J.M., 1998. The effects of particle breakage and abrasion on the magnetic properties of two soils. Hydrol. Process. 12 (9), 1495–1505.
Crockford, R.H., Richardson, D.P., 2004. The Mineral Magnetic Properties of a Multi-Layered Soil in the Australian Captital Territory. Australia, CSIRO Land & Water, Canberra (121 pp).
Crockford, R., Willett, I., 1995. Magnetic-properties of two soils during reduction, drying and re-oxidation. Soil Res. 33 (4), 597–609.
Crockford, R.H., Willett, I.R., 1997. The Magnetic Properties of a Stratigraphic Section of a Sedimentary Soil in New South Wales, Australia. CSIRO Australia, Canberra (142 pp).
Crockford, R.H., Willett, I.R., 2001. Application of mineral magnetism to describe profile development of toposequences of a sedimentary soil in South-Eastern Australia. Soil Res. 39 (5), 927–949.
Cui, Y., Verosub, K.L., Roberts, A.P., 1994. The effect of low-temperature oxidation on large multi-domain magnetite. Geophys. Res. Lett. 21 (9), 757–760.
Dalan, R.A., Banerjee, S.K., 1996. Soil magnetism, an approach for examining archaeological landscapes. Geophys. Res. Lett. 23 (2), 185–188.
Dankoub, Z., Ayoubi, S., Khademi, H., Lu, S.-G., 2012. Spatial distribution of magnetic properties and selected heavy metals in calcareous soils as affected by land use in the Isfahan region, Central Iran. Pedosphere 22 (1), 33–47.
de Caritat, P., Cooper, M., 2011. National Geochemical Survey of Australia: The Geochemical Atlas of Australia. Geoscience Australia Record. (557 pp).
de Caritat, P., Cooper, M., 2016. A continental-scale geochemical atlas for resource exploration and environmental management: the National geochemical survey of Australia. Geochem. Explor. Environ. Anal. 16 (1), 3–13.
Dearing, J.A., 1999. Holocene environmental change from magnetic proxies in lake sediments. In: Quaternary Climates, Environments and Magnetism. Cambridge University Press, Cambridge (231–278 pp).
Dearing, J.A., 2000. Natural magnetic tracers in fluvial geomorphology. In: Tracers in Geomorphology. Wiley, Chichester, pp. 57–82.
Dearing, J.A., Hay, K.L., Baban, S.M.J., Huddleston, A.S., Wellington, E.M.H., Loveland, P.J., 1996. Magnetic susceptibility of soil: an evaluation of conflicting theories using a national data set. Geophys. J. Int. 127 (3), 728–734.
Doetterl, S., Stevens, A., Six, J., Merckx, R., Van Oost, K., Pinto, M.C., Casanova-Katny, A., Munoz, C., Boudin, M., Venegas, E.Z., Boeckx, P., 2015. Soil carbon storage controlled by interactions between geochemistry and climate. Nat. Geosci. 8 (10), 780–783.
Draper, C.S., Walker, J.P., Steinle, P.J., de Jeu, R.A.M., Holmes, T.R.H., 2009. An evaluation of AMSR–E derived soil moisture over Australia. Remote Sens. Environ. 113 (4), 703–710.
Dunlop, D.J., Özdemir, Ö., 1997. Rock Magnetism: Fundamentals and Frontiers. Cambridge University Press, Cambridge (376 pp).
Eggleton, R.A., 2001. Glossary of Regolith-Surficial Geology, Soil and Landscape. CRC LEME Publication, Perth (144 pp).
Egli, R., 2003. Analysis of the field dependence of remanent magnetization curves. J. Geophys. Res. Solid Earth 108 (B2). https://doi.org/10.1029/2002JB002023.
Fassbinder, J.W.E., Stanjek, H., Vali, H., 1990. Occurrence of magnetic bacteria in soil. Nature 343 (6254), 161–163.
Foster, I.D.L., Mighall, T.M., Wotton, C., Owens, P.N., Walling, D.E., 2000. Evidence for mediaeval soil erosion in the south Hams region of Devon, UK. The Holocene 10 (2), 261–271.
Gao, X., Hao, Q., Wang, L., Oldfield, F., Bloemendal, J., Deng, C., Song, Y., Ge, J., Wu, H., Xu, B., Li, F., Han, L., Fu, Y., Guo, Z., 2018. The different climatic response of pedogenic hematite and ferrimagnetic minerals: evidence from particle-sized modern soils over the Chinese Loess Plateau. Quat. Sci. Rev. 179, 69–86.
Ge, K., Williams, W., Liu, Q., Yu, Y., 2014. Effects of the core-shell structure on the magnetic properties of partially oxidized magnetite grains: experimental and micromagnetic investigations. Geochem. Geophys. Geosyst. 15 (5), 2021–2038.
Geiss, C.E., Zanner, C.W., 2007. Sediment magnetic signature of climate in modern loessic soils from the Great Plains. Quat. Int. 162–163, 97–110.
Geiss, C.E., Egli, R., Zanner, C.W., 2008. Direct estimates of pedogenic magnetite as a tool to reconstruct past climates from buried soils. J. Geophys. Res. Solid Earth 113 (B11). https://doi.org/10.1029/2008jb005669.
Goovaerts, P., 1997. Geostatistics for Natural Resources Evaluation. Oxford University Press, New York (483 pp).
Gray, J.M., Humphreys, G.S., Deckers, J.A., 2009. Relationships in soil distribution as revealed by a global soil database. Geoderma 150 (3), 309–323.
Grundy, M.J., Viscarra Rossel, R.A., Searle, R.D., Wilson, P.L., Chen, C., Gregory, L.J., 2015. The soil and landscape grid of Australia. Soil Res. 53 (8), 835–844.
Guo, B., Zhu, R.X., Roberts, A.P., Florindo, F., 2001. Lack of correlation between paleoprecipitation and magnetic susceptibility of Chinese Loess/Paleosol Sequences. Geophys. Res. Lett. 28 (22), 4259–4262.
Han, J.M., Lü, H.Y., Wu, N.Q., Guo, Z.T., 1996. The magnetic susceptibility of modern soils in China and its use for paleoclimate reconstruction. Stud. Geophys. Geod. 40 (3), 262–275.
Hanesch, M., Scholger, R., 2002. Mapping of heavy metal loadings in soils by means of magnetic susceptibility measurements. Environ. Geol. 42 (8), 857–870.
Hanesch, M., Rantitsch, G., Hemetsberger, S., Scholger, R., 2007. Lithological and pedological influences on the magnetic susceptibility of soil: their consideration in magnetic pollution mapping. Sci. Total Environ. 382 (2–3), 351–363.
Hannam, J.A., Dearing, J.A., 2008. Mapping soil magnetic properties in Bosnia and Herzegovina for landmine clearance operations. Earth Planet. Sci. Lett. 274 (3), 285–294.
Hao, Q., Oldfield, F., Bloemendal, J., Torrent, J., Guo, Z., 2009. The record of changing hematite and goethite accumulation over the past 22 Myr on the Chinese Loess Plateau from magnetic measurements and diffuse reflectance spectroscopy. J. Geophys. Res. Solid Earth 114 (B12). https://doi.org/10.1029/2009JB006604.
Hartemink, A.E., Krasilnikov, P., Bockheim, J.G., 2013. Soil maps of the world. Geoderma 207-208, 256–267.
Hatfield, R.G., Maher, B.A., 2008. Suspended sediment characterization and tracing using a magnetic fingerprinting technique: Bassenthwaite Lake, Cumbria, UK. The Holocene 18 (1), 105–115.
Heller, F., Evans, M.E., 1995. Loess magnetism. Rev. Geophys. 33 (2), 211–240.
Hengl, T., Heuvelink, G.B.M., Kempen, B., Leenaars, J.G.B., Walsh, M.G., Shepherd, K.D., Sila, A., MacMillan, R.A., de Jesus, J.M., Tamene, L., Tondoh, J.E., 2015. Mapping soil properties of Africa at 250 m resolution: random forests significantly improve current predictions. PLoS ONE 10 (6). https://doi.org/10.1371/journal.pone.0125814.
Hengl, T., de Jesus, J.M., Heuvelink, G.B.M., Gonzalez, M.R., Kilibarda, M., Blagotic, A., Shangguan, W., Wright, M.N., Geng, X.Y., Bauer-Marschallinger, B., Guevara, M.A., Vargas, R., MacMillan, R.A., Batjes, N.H., Leenaars, J.G.B., Ribeiro, E., Wheeler, I., Mantel, S., Kempen, B., 2017. SoilGrids250m: global gridded soil information based on machine learning. PLoS ONE 12 (2). https://doi.org/10.1371/journal.pone.0169748.
Heslop, D., Roberts, A.P., 2013. Calculating uncertainties on predictions of palaeoprecipitation from the magnetic properties of soils. Glob. Planet. Chang. 110, 379–385.
Hoffmann, V., Knab, M., Appel, E., 1999. Magnetic susceptibility mapping of roadside pollution. J. Geochem. Explor. 66 (1), 313–326.
Hou, B., Frakes, L.A., Alley, N.F., Stamoulis, V., Rowell, A., 2000. Geoscientific signatures of Tertiary palaeochannels and their significance for mineral eploration in the Gawler Craton. MESA J. 19, 36–39.
Hu, P., Liu, Q., Torrent, J., Barrón, V., Jin, C., 2013. Characterizing and quantifying iron oxides in Chinese loess/paleosols: implications for pedogenesis. Earth Planet. Sci. Lett. 369–370, 271–283.
Hu, P.X., Liu, Q.S., Heslop, D., Roberts, A.P., Jin, C.S., 2015. Soil moisture balance and magnetic enhancement in loess-paleosol sequences from the Tibetan Plateau and Chinese Loess Plateau. Earth Planet. Sci. Lett. 409, 120–132.
Hu, P.X., Jiang, Z.X., Liu, Q.S., Heslop, D., Roberts, A.P., Torrent, J., Barrón, V., 2016. Estimating the concentration of aluminum-substituted hematite and goethite using diffuse reflectance spectrometry and rock magnetism: feasibility and limitations. J. Geophys. Res. Solid Earth 121 (6), 4180–4194.
Isbell, R.F., National Committee on Soil and Terrain, 2016. The Australian Soil Classification. Australian Soil and Land Survey Handbooks Series, CSIRO Publishing (152 pp).
Jafari, A., Ayoubi, S., Khademi, H., Finke, P.A., Toomanian, N., 2013. Selection of a taxonomic level for soil mapping using diversity and map purity indices: a case study from an Iranian arid region. Geomorphology 201, 86–97.
Jenny, H., 1941. Factors of Soil Formation - a System of Quantitative Pedology. McGraw-Hill, New York (109 pp).
Ji, J., Chen, J., Balsam, W., Lu, H., Sun, Y., Xu, H., 2004. High resolution hematite/goethite records from Chinese loess sequences for the last glacial-interglacial cycle: rapid climatic response of the East Asian Monsoon to the tropical Pacific. Geophys. Res. Lett. 31 (3). https://doi.org/10.1029/2003GL018975.
Jiang, Z.X., Liu, Q.S., Barrón, V., Torrent, J., Yu, Y.J., 2012. Magnetic discrimination between Al-substituted hematites synthesized by hydrothermal and thermal dehydration methods and its geological significance. J. Geophys. Res. Solid Earth 117. https://doi.org/10.1029/2011JB008605.
Jiang, Z., Liu, Q., Colombo, C., Barrón, V., Torrent, J., Hu, P., 2014. Quantification of Al-goethite from diffuse reflectance spectroscopy and magnetic methods. Geophys. J. Int. 196 (1), 131–144.
Jiang, Z., Liu, Q., Roberts, A.P., Barrón, V., Torrent, J., Zhang, Q., 2018. A new model for transformation of ferrihydrite to hematite in soils and sediments. Geology 46 (11), 987–990.
Johnson, A.K., 2015. Regolith and Associated Mineral Systems of the Eucla Basin, South Australia. PhD thesis. University of Adelaide (277 pp).
Jordanova, N., 2017. Soil Magnetism: Application in Pedology, Environmental Science and Agriculture. Academic Press (466 pp).
Jordanova, D., Grygar, T., Jordanova, N., Petrov, P., 2011a. Palaeoclimatic significance of hematite/goethite ratio in Bulgarian loess-palaeosol sediments deduced by DRS and rock magnetic measurements. In: Petrovský, E., Ivers, D., Harinarayana, T., Herrero-Bervera, E. (Eds.), The Earth's Magnetic Interior. Springer Netherlands, Dordrecht, pp. 399–412.

Jordanova, D., Jordanova, N., Atanasova, A., Tsacheva, T., Petrov, P., 2011b. Soil tillage erosion estimated by using magnetism of soils-a case study from Bulgaria. Environ. Monit. Assess. 183 (1–4), 381–394.
Jordanova, N., Jordanova, D., Petrov, P., 2016. Soil magnetic properties in Bulgaria at a national scale—challenges and benefits. Glob. Planet. Chang. 137, 107–122.
Kletetschka, G., Banerjee, S.K., 1995. Magnetic stratigraphy of Chinese loess as a record of natural fires. Geophys. Res. Lett. 22 (11), 1341–1343.
Koster, R.D., Dirmeyer, P.A., Guo, Z.C., Bonan, G., Chan, E., Cox, P., Gordon, C.T., Kanae, S., Kowalczyk, E., Lawrence, D., Liu, P., Lu, C.H., Malyshev, S., McAvaney, B., Mitchell, K., Mocko, D., Oki, T., Oleson, K., Pitman, A., Sud, Y.C., Taylor, C.M., Verseghy, D., Vasic, R., Xue, Y.K., Yamada, T., Team, G.L.A.C.E., 2004. Regions of strong coupling between soil moisture and precipitation. Science 305 (5687), 1138–1140.
Krasilnikov, P., Martí, J.J., Arnold, R., Shoba, S., 2009. A Handbook of Soil Terminology, Correlation and Classification. Routledge, London (448 pp).
Larrasoaña, J.C., Roberts, A.P., Rohling, E.J., Winklhofer, M., Wehausen, R., 2003. Three million years of monsoon variability over the northern Sahara. Clim. Dyn. 21 (7–8), 689–698.
Le Borgne, E., 1955. Susceptibilité magnetique anormale du sol superficiel. Annales de Géophysique 11 (399–149).
Le Borgne, E., 1960. Influence du feu sur les propriétés magnétique du sol et sur celles du schiste et du granit. Annales de Géophysique 16, 159–195.
Lee, C.S.-L., Li, X., Shi, W., Cheung, S.C.-N., Thornton, I., 2006. Metal contamination in urban, suburban, and country park soils of Hong Kong: a study based on GIS and multivariate statistics. Sci. Total Environ. 356 (1), 45–61.
Li, Q., Kartikowati, C.W., Horie, S., Ogi, T., Iwaki, T., Okuyama, K., 2017. Correlation between particle size/domain structure and magnetic properties of highly crystalline Fe_3O_4 nanoparticles. Sci. Rep. 7 (1). https://doi.org/10.1038/s41598-017-09897-5.
Liu, Q., Banerjee, S.K., Jackson, M.J., Chen, F., Pan, Y., Zhu, R., 2003. An integrated study of the grain-size-dependent magnetic mineralogy of the Chinese loess/paleosol and its environmental significance. J. Geophys. Res. Solid Earth 108 (B9). https://doi.org/10.1029/2002JB002264.
Liu, Q.S., Deng, C.L., Torrent, J., Zhu, R.X., 2007. Review of recent developments in mineral magnetism of the Chinese loess. Quat. Sci. Rev. 26 (3–4), 368–385.
Liu, Q.S., Barrón, V., Torrent, J., Eeckhout, S.G., Deng, C.L., 2008. Magnetism of intermediate hydromaghemite in the transformation of 2-line ferrihydrite into hematite and its paleoenvironmental implications. J. Geophys. Res. Solid Earth 113 (B1). https://doi.org/10.1029/2007jb005207.
Liu, Q.S., Hu, P.X., Torrent, J., Barrón, V., Zhao, X.Y., Jiang, Z.X., Su, Y.L., 2010. Environmental magnetic study of a Xeralf chronosequence in northwestern Spain: indications for pedogenesis. Palaeogeogr. Palaeoclimatol. Palaeoecol. 293 (1–2), 144–156.
Liu, Q., Roberts, A.P., Larrasoaña, J.C., Banerjee, S.K., Guyodo, Y., Tauxe, L., Oldfield, F., 2012. Environmental magnetism: principles and applications. Rev. Geophys. 50 (4). https://doi.org/10.1029/2012RG000393.
Liu, Z., Liu, Q., Torrent, J., Barrón, V., Hu, P., 2013. Testing the magnetic proxy χ_{FD}/HIRM for quantifying paleoprecipitation in modern soil profiles from Shaanxi Province, China. Glob. Planet. Chang. 110, 368–378.
Liu, Q.S., Sun, Y.B., Qiang, X.K., Tada, R.J., Hu, P.X., Duan, Z.Q., Jiang, Z.X., Liu, J.X., Su, K., 2015. Characterizing magnetic mineral assemblages of surface sediments from major Asian dust sources and implications for the Chinese loess magnetism. Earth Planets Space 67, 1–17.
Long, X., Ji, J., Balsam, W., 2011. Rainfall-dependent transformations of iron oxides in a tropical saprolite transect of Hainan Island, South China: spectral and magnetic measurements. J. Geophys. Res. Earth Surf. 116 (F3). https://doi.org/10.1029/2010JF001712.
Lowry, D.C., 1971. Geology of the Western Australia part of the Eucla Basin. Geol. Surv. W. Aust. Bull. 112, 200.
Lyons, R., Oldfield, F., Williams, E., 2010. Mineral magnetic properties of surface soils and sands across four North African transects and links to climatic gradients. Geochem. Geophys. Geosyst. 11 (8). https://doi.org/10.1029/2010GC003183.
Lyons, R., Tooth, S., Duller, G.A.T., 2014. Late Quaternary climatic changes revealed by luminescence dating, mineral magnetism and diffuse reflectance spectroscopy of river terrace palaeosols: a new form of geoproxy data for the southern African interior. Quat. Sci. Rev. 95, 43–59.
Ma, M., Liu, X., Hesse, P.P., Lü, B., Guo, X., Chen, J., 2013. Magnetic properties of loess deposits in Australia and their environmental significance. Quat. Int. 296, 198–205.
Maher, B.A., 1986. Characterisation of soils by mineral magnetic measurements. Phys. Earth Planet. Inter. 42 (1), 76–92.
Maher, B.A., 1998. Magnetic properties of modern soils and Quaternary loessic paleosols: paleoclimatic implications. Palaeogeogr. Palaeoclimatol. Palaeoecol. 137 (1–2), 25–54.
Maher, B.A., 2011. The magnetic properties of Quaternary aeolian dusts and sediments, and their palaeoclimatic significance. Aeolian Res. 3 (2), 87–144.
Maher, B.A., Possolo, A., 2013. Statistical models for use of palaeosol magnetic properties as proxies of palaeorainfall. Glob. Planet. Chang. 111, 280–287.
Maher, B.A., Taylor, R.M., 1988. Formation of ultrafine-grained magnetite in soils. Nature 336 (6197), 368–370.
Maher, B.A., Thompson, R., 1992. Paleoclimatic significance of the mineral magnetic record of the Chinese loess and paleosols. Quat. Res. 37 (2), 155–170.
Maher, B.A., Thompson, R., 1995. Paleorainfall reconstructions from pedogenic magnetic susceptibility variations in the Chinese loess and paleosols. Quat. Res. 44 (3), 383–391.
Maher, B.A., Thompson, R., Zhou, L.P., 1994. Spatial and temporal reconstructions of changes in the Asian palaeomonsoon - a new mineral magnetic approach. Earth Planet. Sci. Lett. 125 (1–4), 461–471.
Maher, B.A., Alekseev, A., Alekseeva, T., 2002. Variation of soil magnetism across the Russian steppe: its significance for use of soil magnetism as a palaeorainfall proxy. Quat. Sci. Rev. 21 (14–15), 1571–1576.
Maher, B.A., Alekseev, A., Alekseeva, T., 2003. Magnetic mineralogy of soils across the Russian Steppe: climatic dependence of pedogenic magnetite formation. Palaeogeogr. Palaeoclimatol. Palaeoecol. 210 (3–4), 321–341.
Manjoro, M., Rowntree, K., Kakembo, V., Foster, I., Collins, A.L., 2017. Use of sediment source fingerprinting to assess the role of subsurface erosion in the supply of fine sediment in a degraded catchment in the Eastern Cape, South Africa. J. Environ. Manag. 194, 27–41.
Martin, A.P., Ohneiser, C., Turnbull, R.E., Strong, D.T., Demler, S., 2018. Soil magnetic susceptibility mapping as a pollution and provenance tool: an example from southern New Zealand. Geophys. J. Int. 212 (2), 1225–1236.
Maxbauer, D.P., Feinberg, J.M., Fox, D.L., 2016. Magnetic mineral assemblages in soils and paleosols as the basis for paleoprecipitation proxies: a review of magnetic methods and challenges. Earth Sci. Rev. 155, 28–48.
Maxbauer, D.P., Feinberg, J.M., Fox, D.L., Nater, E.A., 2017. Response of pedogenic magnetite to changing vegetation in soils developed under uniform climate, topography, and parent material. Sci. Rep. 7 (1). https://doi.org/10.1038/s41598-017-17722-2.
McBratney, A.B., Webster, R., 1986. Choosing functions for semi-variograms of soil properties and fitting them to sampling estimates. J. Soil Sci. 37 (4), 617–639.
McBratney, A.B., Mendonça Santos, M.L., Minasny, B., 2003. On digital soil mapping. Geoderma 117 (1), 3–52.
McColl, K.A., Alemohammad, S.H., Akbar, R., Konings, A.G., Yueh, S., Entekhabi, D., 2017. The global distribution and dynamics of surface soil moisture. Nat. Geosci. 10 (2), 100–104.
Michel, F.M., Barrón, V., Torrent, J., Morales, M.P., Serna, C.J., Boily, J.F., Liu, Q.S., Ambrosini, A., Cismasu, A.C., Brown, G.E., 2010. Ordered ferrimagnetic form of ferrihydrite reveals links among structure, composition, and magnetism. Proc. Natl. Acad. Sci. U. S. A. 107 (7), 2787–2792.
Mokhtari Karchegani, P., Ayoubi, S., Lu, S.G., Honarju, N., 2011. Use of magnetic measures to assess soil redistribution following deforestation in hilly region. J. Appl. Geophys. 75 (2), 227–236.
Moteki, N., Adachi, K., Ohata, S., Yoshida, A., Harigaya, T., Koike, M., Kondo, Y., 2017. Anthropogenic iron oxide aerosols enhance atmospheric heating. Nat. Commun. 8. https://doi.org/10.1038/ncomms15329.
Mullins, C.E., 1977. Magnetic-susceptibility of soil and its significance in soil science - review. J. Soil Sci. 28 (2), 223–246.
Naimi, S., Ayoubi, S., 2013. Vertical and horizontal distribution of magnetic susceptibility and metal contents in an industrial district of Central Iran. J. Appl. Geophys. 96, 55–66.
Oldfield, F., Crowther, J., 2007. Establishing fire incidence in temperate soils using magnetic measurements. Palaeogeogr. Palaeoclimatol. Palaeoecol. 249 (3–4), 362–369.
Oliver, M.A., Webster, R., 2014. A tutorial guide to geostatistics: computing and modelling variograms and kriging. Catena 113, 56–69.
Orgeira, M.J., Egli, R., Compagnucci, R.H., 2011. A quantitative model of magnetic enhancement in loessic soils. In: Petrovský, E., Ivers, D., Harinarayana, T., Herrero-Bervera, E. (Eds.), The Earth's Magnetic Interior. Springer Netherlands, Dordrecht, pp. 361–397.
Orgiazzi, A., Ballabio, C., Panagos, P., Jones, A., Fernández-Ugalde, O., 2018. LUCAS Soil, the largest expandable soil dataset for Europe: a review. Eur. J. Soil Sci. 69 (1), 140–153.
Otrakdjian, L., Keeling, J., 2010. Jacinth-Ambrosia heavy mineral sands mine: discovery to production. MESA J. 5, 5–9.
Pain, C.F., Pillans, B.J., Roach, I.C., Worrall, L., Wilford, J., 2012. Old, flat and red - Australia's distinctive landscape. In: Blewett, R. (Ed.), Shaping a Nation - A Geology of Australia. ANU press, Canberra.
Paterson, G.A., Heslop, D., 2015. New methods for unmixing sediment grain size data. Geochem. Geophys. Geosyst. 16 (12), 4494–4506.
Paustian, K., Lehmann, J., Ogle, S., Reay, D., Robertson, G.P., Smith, P., 2016. Climate-smart soils. Nature 532 (7597), 49–57.
Pillans, B., 2009. Regolith through time. In: Scott, K.M., Pain, C.F. (Eds.), Regolith Science. CSIRO Publishing, Australia, pp. 472.
Pulley, S., Collins, A.L., Van der Waal, B., 2018. Variability in the mineral magnetic properties of soils and sediments within a single field in the Cape Fold mountains, South Africa: implications for sediment source tracing. Catena 163, 172–183.
Rachwał, M., Kardel, K., Magiera, T., Bens, O., 2017. Application of magnetic susceptibility in assessment of heavy metal contamination of Saxonian soil (Germany) caused by industrial dust deposition. Geoderma 295, 10–21.
Roberts, A.P., 2015. Magnetic mineral diagenesis. Earth Sci. Rev. 151, 1–47.
Sacristán, D., Viscarra Rossel, R.A., Recatalá, L., 2016. Proximal sensing of Cu in soil and lettuce using portable X-ray fluorescence spectrometry. Geoderma 265, 6–11.
Sadiki, A., Faleh, A., Navas, A., Bouhlassa, S., 2009. Using magnetic susceptibility to assess soil degradation in the Eastern Rif, Morocco. Earth Surf. Process. Landf. 34 (15), 2057–2069.
Singer, M.J., Verosub, K.L., Fine, P., TenPas, J., 1996. A conceptual model for the enhancement of magnetic susceptibility in soils. Quat. Int. 34–6, 243–248.
Singh, B., Gilkes, R.J., 1992. Properties and distribution of iron-oxides and their association with minor elements in the soils of South-Western Australia. J. Soil Sci. 43 (1), 77–98.
Thompson, R., Oldfield, F., 1986. Environmental Magnetism. Allen and Unwin, London, UK (227 pp).
Torrent, J., Schwertmann, U., Schulze, D.G., 1980. Iron-oxide mineralogy of some soils of 2 river terrace sequences in Spain. Geoderma 23 (3), 191–208.

Torrent, J., Barrón, V., Liu, Q.S., 2006. Magnetic enhancement is linked to and precedes hematite formation in aerobic soil. Geophys. Res. Lett. 33 (2). https://doi.org/10.1029/2005gl024818.
Torrent, J., Liu, Q.S., Bloemendal, J., Barrón, V., 2007. Magnetic enhancement and iron oxides in the upper Luochuan loess-paleosol sequence, Chinese loess plateau. Soil Sci. Soc. Am. J. 71 (5), 1570–1578.
Torrent, J., Liu, Q.S., Barrón, V., 2010. Magnetic susceptibility changes in relation to pedogenesis in a Xeralf chronosequence in northwestern Spain. Eur. J. Soil Sci. 61 (2), 161–173.
van Velzen, A.J., Dekkers, M.J., 1999. Low-temperature oxidation of magnetite in loess-paleosol sequences: a correction of rock magnetic parameters. Stud. Geophys. Geod. 43 (4), 357–375.
Viscarra Rossel, R.A., 2011. Fine-resolution multiscale mapping of clay minerals in Australian soils measured with near infrared spectra. J. Geophys. Res. Earth Surf. 116 (F4). https://doi.org/10.1029/2011JF001977.
Viscarra Rossel, R.A., Webster, R., 2012. Predicting soil properties from the Australian soil visible–near infrared spectroscopic database. Eur. J. Soil Sci. 63 (6), 848–860.
Viscarra Rossel, R.A., Bui, E.N., de Caritat, P., McKenzie, N.J., 2010. Mapping iron oxides and the color of Australian soil using visible–near-infrared reflectance spectra. J. Geophys. Res. Earth Surf. 115 (F4). https://doi.org/10.1029/2009JF001645.
Viscarra Rossel, R.A., Webster, R., Bui, E.N., Baldock, J.A., 2014. Baseline map of organic carbon in Australian soil to support national carbon accounting and monitoring under climate change. Glob. Chang. Biol. 20 (9), 2953–2970.
Viscarra Rossel, R.A., Chen, C., Grundy, M.J., Searle, R., Clifford, D., Campbell, P.H., 2015. The Australian three-dimensional soil grid: Australia's contribution to the GlobalSoilMap project. Soil Res. 53 (8), 845–864.
Viscarra Rossel, R.A., Behrens, T., Ben-Dor, E., Brown, D.J., Dematte, J.A.M., Shepherd, K.D., Shi, Z., Stenberg, B., Stevens, A., Adamchuk, V., Aichi, H., Barthes, B.G., Bartholomeus, H.M., Bayer, A.D., Bernoux, M., Bottcher, K., Brodsky, L., Du, C.W., Chappell, A., Fouad, Y., Genot, V., Gomez, C., Grunwald, S., Gubler, A., Guerrero, C., Hedley, C.B., Knadel, M., Morras, H.J.M., Nocita, M., Ramirez-Lopez, L., Roudier, P., Campos, E.M.R., Sanborn, P., Sellitto, V.M., Sudduth, K.A., Rawlins, B.G., Walter, C., Winowiecki, L.A., Hong, S.Y., Ji, W., 2016. A global spectral library to characterize the world's soil. Earth Sci. Rev. 155, 198–230.
Viscarra Rossel, R.A., Lee, J., Behrens, T., Luo, Z., Baldock, J., Richards, A., 2019. Continental-scale soil carbon composition and vulnerability modulated by regional environmental controls. Nat. Geosci. 12 (7), 547–552.
Wilford, J., 2012. A weathering intensity index for the Australian continent using airborne gamma-ray spectrometry and digital terrain analysis. Geoderma 183, 124–142.
Wilford, J., de Caritat, P., Bui, E., 2015. Modelling the abundance of soil calcium carbonate across Australia using geochemical survey data and environmental predictors. Geoderma 259-260, 81–92.
Zamanian, K., Pustovoytov, K., Kuzyakov, Y., 2016. Pedogenic carbonates: forms and formation processes. Earth Sci. Rev. 157, 1–17.
Zeraatpisheh, M., Ayoubi, S., Jafari, A., Finke, P., 2017. Comparing the efficiency of digital and conventional soil mapping to predict soil types in a semi-arid region in Iran. Geomorphology 285, 186–204.